



# NASA Contractor Report 159004

NASA-CR-159004

19790009624

EXPERIMENTAL INVESTIGATION OF JET-INDUCED LOADS  
ON A FLAT PLATE IN HOVER OUT-OF-GROUND EFFECT

John M. Kuhlman and Ronald W. Warcup

OLD DOMINION UNIVERSITY RESEARCH FOUNDATION  
Norfolk, Virginia 23508

NASA Contract NAS1-14193-Task 40  
February 1979

**LIBRARY COPY**

FEB 20 1979

LANGLEY RESEARCH CENTER  
LIBRARY, NASA  
HAMPTON, VIRGINIA



National Aeronautics and  
Space Administration

**Langley Research Center**  
Hampton, Virginia 23665



NF01321

## TABLE OF CONTENTS

	<u>Page</u>
SUMMARY . . . . .	1
INTRODUCTION . . . . .	1
SYMBOLS . . . . .	2
APPARATUS . . . . .	3
EXPERIMENTAL PROCEDURE . . . . .	4
RESULTS . . . . .	7
DISCUSSION OF RESULTS . . . . .	8
CONCLUSIONS . . . . .	10
APPENDIX A: NOZZLE CALIBRATION DATA FOR JET IN HOVER . . . . .	22
APPENDIX B: TABULATED JET-IN-HOVER DYNAMIC PRESSURE DECAY DATA . . . . .	33
APPENDIX C: TABULATED STATIC PRESSURE DATA FOR JET IN HOVER . . . . .	42
REFERENCES . . . . .	60

## LIST OF FIGURES

### Figure

1. Experimental apparatus . . . . .	11
2. Flat plate pressure port distribution . . . . .	12
3. Cross section of jet nozzle, plenum, and centerbody . . . . .	13
4. Nondimensional lift loss, $\Delta L/T$ , for round-tipped plug configurations in hover compared with unplugged jet . . . . .	14
5. Jet centerline dynamic pressure decay for round-tipped plug configurations in hover compared with unplugged jet . . . . .	15
6. Nondimensional lift loss, $\Delta L/T$ , for flat-tipped plug configurations in hover compared with unplugged jet . . . . .	16
7. Jet centerline dynamic pressure decay for flat-tipped plug configurations in hover compared with unplugged jet . . . . .	17

<u>Figure</u>		<u>Page</u>
8.	Comparison of induced lift loss for jet in hover with results of reference 5 . . . . .	18
9.	Comparison of dynamic pressure decay for jet in hover with results of reference 5 . . . . .	19
10.	Logarithmic replot of hover jet dynamic pressure decay data; no plug and round plug configurations . . . . .	20
11.	Logarithmic replot of hover jet dynamic pressure decay data; no plug and flat plug configurations . . . . .	21

EXPERIMENTAL INVESTIGATION OF JET-INDUCED LOADS  
ON A FLAT PLATE IN HOVER OUT-OF-GROUND EFFECT

By

John M. Kuhlman and Ronald W. Warcup  
Old Dominion University

SUMMARY

Effects of varying jet decay rate on jet-induced loads on a flat plate located in the plane of the jet exit perpendicular to the jet axis have been investigated using a small-scale laboratory facility. Jet decay rate has been varied through use of two cylindrical centerbodies having either a flat or hemispherical tip, which were submerged various distances below the flat plate-jet exit plane. Increased jet decay rate, caused by the presence of a centerbody or plug in the jet nozzle, led to an increased jet-induced lift loss on the flat plate. Jet-induced lift losses reached 1 percent of the jet thrust for the quickest jet decay rates for plate areas equal to 100 times the effective jet exit area. The observed lift loss versus jet decay rate trend agreed well with results of previous investigations.

INTRODUCTION

Accurate prediction of jet-induced loads on a jet VTOL aircraft under a variety of flight conditions is quite important in achieving aircraft design performance goals. Many previous studies have indicated quite a range of possible loadings, depending upon jet nozzle geometry or the number of jet nozzles (refs. 1-4) or jet decay rate (refs. 5,6). Gentry and Margason (ref. 5) found that the jet-induced lift loss increased as the jet decay rate increased for a single jet in hover issuing perpendicular to a circular flat plate. However, Kuhlman et al. (refs. 6-8) found an opposite trend for a similar jet subjected to a crossflow. That is, as jet decay rate was increased for a jet in a crossflow, results indicated that the jet-induced lift loss decreased for a fixed ratio of jet-to-crossflow velocities.

Therefore, the current study was undertaken using essentially the same experimental apparatus of references 6 through 8 to determine if these hardware produce hover lift-induced effects consistent with the hover results of Gentry and Margason.

#### SYMBOLS

Results are presented in nondimensional coefficient form, or, where appropriate, in both SI Units and U. S. Customary Units. Data has generally been taken and calculations made in U. S. Customary Units.

A	area on the flat plate, $m^2$ ( $ft^2$ )
$A_e$	effective jet exit area, $m^2$ ( $ft^2$ ); see equation (3)
$D_e$	effective jet exit diameter, m (ft); $D_e = \sqrt{4A_e/\pi}$
$D_n$	nominal jet exit diameter (jet orifice diameter), m (ft)
$\Delta L$	jet-induced lift loss, N (lb)
$\dot{m}$	jet mass flow rate, kg/sec (slug/sec)
p	static pressure, $N/m^2$ ( $lb/ft^2$ )
$p_e$	jet exit static pressure, $N/m^2$ ( $lb/ft^2$ )
Q	volume flow rate, $m^3/sec$ (CFM)
q	dynamic pressure, $N/m^2$ ( $lb/ft^2$ )
$q_{max}$	maximum exit plane dynamic pressure, $N/m^2$ ( $lb/ft^2$ )
R	gas constant, Joule/kg-K ( $ft\text{-}lb/slug\text{-}R$ )
r	radius, m (ft)
T	jet thrust, N (lb)
$T_e$	jet exit static temperature, K (R)
$V_e$	effective jet exit velocity, m/s ( $ft/s$ ); see equation (4)
x	coordinate along longer dimension of plate, origin at center of jet orifice, m (ft)
y	coordinate along shorter dimension of plate, origin at center of jet orifice, m (ft)

z coordinate perpendicular to plate, origin at center of jet orifice, m (ft)  
γ ratio of specific heats  
ρ density, kg/m<sup>3</sup> (slug/ft<sup>3</sup>)

Subscripts:

e effective; exit  
max maximum  
n nominal

APPARATUS

The work reported herein was performed using the same flat plate, nozzle and transducers used in references 6, 7, and 8. The flat plate was made from hard board sheet 0.905-m (36-D<sub>n</sub>) wide by 1.22-m (48-D<sub>n</sub>) long. The plate was 1.90-cm (0.75-in.) thick, fitted with a round leading edge and a tapered trailing edge. For this study, the plate was mounted between two laboratory tables 0.80 m (2.63 ft) from the floor. A view of the flat plate used in this work appears in figure 1. The 1.45-m (4.75-ft) diameter by 0.91-m (3-ft) high circular screen of mesh size 1.6 mm (0.063 in.) was placed symmetrically around the plate to damp out disturbances in the entrained jet flow due to room pressure variations caused by the opening or closing of building doors. The laboratory ceiling was 4.3 m (14 ft) above the plane of the flat plate. The plate was fitted with 226 static pressure taps located on rays emanating from the jet orifice center as shown in figure 2. These pressure ports were made from 0.61-mm diameter stainless steel tubing. Distances from the nozzle centerline to the various pressure tap locations are listed in table C1 (Appendix C). The plate surface was smoothed and filled with epoxy, resulting in the removal of an elliptical low region in the plate around the jet, which was created by continual polishing and smoothing of the plate during previous studies (refs. 6-8). This was necessary to insure a symmetrical pressure distribution on the plate surface.

The jet exited perpendicular to the plate through a circular orifice 2.54 cm (1.0 in.) in diameter. The nozzle center was located 0.6 m (2 ft) from the rounded edge of the plate halfway across the 0.915-m dimension of the plate. The air jet issued from a 0.14-m (0.466-ft) diameter plenum chamber supplied by an air compressor through a smoothly contoured 30:1 area ratio contraction nozzle. A sectional view of the plenum and nozzle is shown in figure 3. Jet mass flow rate was measured with a turbine type flowmeter and held constant to within  $\pm 0.2$  percent during any one run using an electronic feedback control. The only difference between the current apparatus and that used in references 6 to 8 was a machined nozzle exit, fitted to the original nozzle, which was longer than the original nozzle.

Also shown in figure 3 is one of the two centerbodies, or plugs, used to vary the jet exit plane dynamic pressure profiles, and hence jet decay rate. The centerbody shown is cylindrical with a diameter of 1.9 cm (0.75 in. or  $0.75 D_n$ ), fitted with a hemispherical tip pointed in the jet flow direction. This centerbody is referred to as a round-ended plug in this report. A second centerbody or plug of the same diameter having a flat end has also been used in some data runs. Jet decay rate has been altered by varying the submergence depth of the tips of these plugs beneath the jet exit-flat plate plane.

The plate surface static pressure ports were connected by plastic tubing and four scanning valves to a single capacitance type pressure transducer, digital electronic manometer, and chart recorder. Pressure transducers were calibrated using a dead weight tester.

A two degrees of freedom traverse fitted with a 1.6-mm (0.0625-in.) diameter pitot static probe was clamped to a corner of the flat plate to measure jet dynamic pressures. Temperatures of the jet and ambient air were monitored by 0.25-mm diameter chromel alumel thermocouples. Room air temperature was nominally 294 K (530 R), with jet exit temperatures nominally within 1 K (2 R) of the ambient temperature.

#### EXPERIMENTAL PROCEDURE

The jet nozzle and plenum were physically aligned to be at right angles to the plate and were then rigidly mounted to the plate. This insured axial

symmetry of the jet-induced plate static pressure distribution for a jet configuration with no centerbody. For nozzle configurations with a centerbody, the centerbody was first aligned mechanically with respect to the flat plate and nozzle, and then if necessary adjusted slightly to yield both a symmetrical jet exit plane dynamic pressure distribution and a symmetrical plate surface pressure distribution. Jet exit plane dynamic pressure profiles were measured using the pitot static probe located  $0.25 D_n$  above the jet exit plane. Air flow rates for each nozzle-centerbody configuration were adjusted so that maximum jet exit dynamic pressures,  $q_{max}$ , were held nearly constant. Maximum jet exit Mach number was nominally 0.4, and Reynolds number based on  $q_{max}$  and  $D_n$  was  $2 \times 10^5$ . Jet exit dynamic pressure profiles were similar to those obtained in references 6, 7, and 8.

For the various nozzle-centerbody configurations calibrated as described above and in Appendix A, the jet centerline dynamic pressure decay was measured using the pitot static probe and traverse. Also, for each of these nozzle-centerbody configurations, the jet-induced static pressures on the plate surface were measured using the pressure transducer, manometer, and recorder. Pressures were electrically integrated nominally for five seconds, and the resulting integrated pressure values were then averaged circumferentially at each radial pressure port location. Average pressure values at any radial station varied by no more than five percent for all circumferential stations. It is believed that much of this variation was the result of slight imperfections in the radial locations of some pressure ports and irregularities in the plate surface.

Jet thrust,  $T$ , has been calculated through use of the measured exit plane dynamic pressure profiles. A procedure somewhat different from, but related to that developed by Ziegler and Wooler (ref. 4) and used by the authors in references 6, 7, and 8, was used in this study. Previously, a jet thrust,  $T$ , was calculated from integration of the jet exit plane dynamic pressure profiles, and  $T$  was used to calculate an effective jet exit dynamic pressure from

$$q_{eff} = \frac{P_e \left( \frac{T}{\dot{m}} \right)^2}{2RT_e - \frac{\gamma - 1}{\gamma} \left( \frac{T}{\dot{m}} \right)^2} \quad (1)$$



In this study the maximum observed exit plane dynamic pressure,  $q_{\max}$ , was used to estimate the jet thrust,  $T$ , from equation (1). Solving for  $T$  gives

$$T = \dot{m} \sqrt{\frac{2RT_e q_{\max}}{P_e + \frac{\gamma - 1}{\gamma} q_{\max}}} \quad (2)$$

This calculated thrust has been used to nondimensionalize all measured lift losses,  $\Delta L$ . The effective jet area used to calculate the reference length,  $D_e$ , used to nondimensionalize all distances, has been calculated by

$$A_e = T / (2q_{\max}). \quad (3)$$

It is estimated that this procedure gives results which lie within 10 percent of those obtained using the earlier procedure of references 6 through 8. Differences are due to inaccuracies in the measured  $q$  distributions near the jet exit near the nozzle or centerbody wall, as discussed in reference 7. It is believed that the  $q$  distributions have been greatly altered due to a blockage effect of the probe which is particularly noticeable for the flat plug flush configuration. Also, the measured  $q$  distributions have been smeared or averaged radially by the pitot static probe, whose diameter was one-half the annular gap between the nozzle and centerbody. All data for the various nozzle-centerbody configurations have been obtained holding the effective jet exit velocity,  $V_e$ , fixed where

$$V_e = \frac{\dot{m}}{\rho_e A_e} \quad (4)$$

and  $\dot{m}$  has been measured with a turbine flowmeter. The data-reduction procedure used in this study was adopted because it yields results which are more self-consistent than those found by the earlier method (refs. 6-8). For example, the value of  $A_e$  calculated using this procedure from equations (2) and (3) for the flat-ended plug flush configuration is very close to the actual physical exit area. However, use of equations (1) and (3), as in the

earlier references, for this configuration would result in a value of  $A_e$  25 percent larger than the actual area.

## RESULTS

Jet dynamic pressure decay data and jet-induced pressure distribution data have been obtained for the following jet-in-hover, nozzle-centerbody-plate configurations:

- (1) no centerbody;
- (2) hemispherical-tipped centerbody flush with jet exit plane;
- (3) hemispherical-tipped centerbody submerged  $1.0 D_n$  below jet exit plane;
- (4) hemispherical-tipped centerbody submerged  $0.5 D_n$  below jet exit plane;
- (5) flat-ended centerbody flush with jet exit plane;
- (6) flat-ended centerbody submerged  $0.375 D_n$  below jet exit plane;
- (7) flat-ended centerbody submerged  $0.875 D_n$  below jet exit plane; and
- (8) flat-ended centerbody submerged  $1.375 D_n$  below jet exit plane.

These centerbody shapes and locations are the same as those studied in references 6 through 8. Results are presented in the following figures:

<u>Data</u>	<u>Figure</u>
Integrated jet-induced loads for round-plug and no-plug configurations	4
Jet dynamic pressure decay for round-plug and no-plug configurations	5
Integrated jet-induced loads for flat-plug and no-plug configurations	6
Jet dynamic pressure decay for flat-plug and no-plug configurations	7
Comparisons of current results with those of reference 5	8,9
Logarithmic jet decay data plots	10,11

The measured jet exit plane dynamic pressure profiles are displayed in Appendix A. Table A1 gives the nozzle calibration data for all configurations tested. Tabulated jet decay data for all configurations appears in Appendix B, and tables of plate surface pressures for all jet nozzle configurations tested are given in Appendix C.

## DISCUSSION OF RESULTS

As shown in figures 4 and 6, the presence and location of the centerbodies greatly altered the magnitudes of the jet-induced loads. Figures 5 and 7 show that the jet dynamic pressure decay rates were also altered by the two centerbodies.

Comparison of figures 4 and 5 reveals that there was nearly a one-to-one correspondence or ranking between the round-ended plug configurations having both quicker jet decay rates and larger nondimensional integrated loads,  $\Delta L/T$ . Jet decay rates have been compared based on the  $q(z)$  data for  $z \geq 5$ . The round plug flush configuration had a quicker jet decay rate than the no-plug configuration, and also had a larger nondimensional jet-induced lift loss,  $\Delta L/T$ . This was followed by the round plug submerged  $1.0 D_n$  below the exit plane, with the round plug submerged  $0.5 D_n$  having both the quickest jet decay and the largest  $\Delta L/T$  values for all round-ended plug configurations. Note the crossover of the decay data at  $z/D_e \approx 4$  for the  $1.0 D_n$  and  $0.5 D_n$  configurations.

Study of figures 6 and 7 shows a similar ranking of the various flat-ended centerbody configurations. The flat plug submerged  $1.375 D_n$  displayed the quickest decay rate, but had a slightly smaller  $\Delta L/T$  than the flat plug submerged  $0.875 D_n$  configuration. However, these two runs were followed, in order of both magnitude of  $\Delta L/T$  and decreasing jet decay rate, by the flat plug down  $0.375 D_n$  and the flat plug flush configurations. The decay of the flat plug flush case occurred more quickly than for the no-plug configuration, and it also had a larger  $\Delta L/T$ .

Thus, all data consistently showed for a single jet in hover that an increase in jet decay rate led to a larger nondimensional jet-induced lift loss,  $\Delta L/T$ . This trend is consistent with the earlier results of Gentry and Margason (ref. 5).

While for the flat plug an increase in jet decay rate always corresponded to the plug tip's being submerged further below the jet exit, very little difference was observed in decay rates of the round plug submerged  $1.0 D_n$  or  $0.5 D_n$  configurations.

The observed trend of increased  $\Delta L/T$  for an increased jet decay rate for jets in hover was opposite to the results of references 6, 7, and 8 for a jet in a uniform crossflow. Using nearly the same apparatus as that used in this study, it was found during the earlier work that quicker jet decay rates for a jet in a crossflow led to a decrease in  $\Delta L/T$ .

Lift losses for a jet in a crossflow were on the order of 50 times larger, relative to the jet thrust, than corresponding  $\Delta L/T$  values found in this study for the hover case. These larger lift losses would be offset by aerodynamic lift or proper configuring of an actual jet VTOL aircraft. Lift losses in hover, on the other hand, could only be compensated for by installation of a larger engine. These lift losses in hover can have a significant effect on the performance of an actual jet VTOL configuration, as discussed in reference 9.

Explanation of the two opposite trends may be achieved by consideration of the different physical mechanisms governing jet development. For a jet in hover, the jet decay is determined solely by turbulent mixing of the jet with the ambient fluid, resulting in entrainment of the ambient into the jet. The resulting inflow velocities, which increase as the jet axis is approached, cause the low-pressure region on the plate around the jet. Hence, in hover quicker jet decay, corresponding to better turbulent mixing, leads to increased entrained inflow and an increased lift loss.

However, for a similar jet configuration in a crossflow, there are two other mechanisms governing the jet-induced loading on the plate. First, the jet acts somewhat like a solid obstruction to the crossflow, causing a small positive pressure region on the plate ahead of the jet (refs. 6, 8, 10, and 11). This positive pressure region increases as the crossflow velocity increases. Second, and most importantly, the crossflow jet flow field is dominated by a contrarotating vortex pair located somewhat above the jet centerline, which is formed as the crossflow flows around the jet, as documented by Kamotani and Greber in reference 12. It is this organized vortex pair which dominates

jet entrainment, and hence jet-induced loads, for a jet in a crossflow. References 6 and 8 further concluded that the presence of a centerbody in the jet nozzle, while leading to quicker jet centerline dynamic pressure decay, lead also to a weakening of the vortex pair, and hence to a decreased  $\Delta L/T$ .

In figures 8 and 9 the current results are compared with results of reference 5 using a different apparatus. Although the apparatus used was different, the resulting lift loss and decay rate trends agree well with results from this study. Lift losses for a jet in hover are at most 1 percent of jet thrust for a plate area equal to 100 jet exit areas. In figures 10 and 11, the current decay data have been replotted on logarithmic axes. It is seen that all jet decay rates have been altered largely by changing the length of the flow establishment region near the jet exit.

#### CONCLUSIONS

The jet centerline dynamic pressure decay rate and jet-induced load data derived in this study for a single jet issuing at right angles to a flat plate into still air (hover case) have shown that:

- (1) The presence of a centerbody in the jet nozzle and plenum leads to nonuniform jet exit plane dynamic pressure profiles and alters the jet centerline dynamic pressure decay rate;
- (2) More rapid jet dynamic pressure decay corresponds to a larger jet-induced lift loss on the flat plate, consistent with results of Gentry and Margason (ref. 5), and
- (3) These jet-induced lift losses are typically on the order of 1 percent of the jet thrust for a plate area equal to 100 times the jet exit area

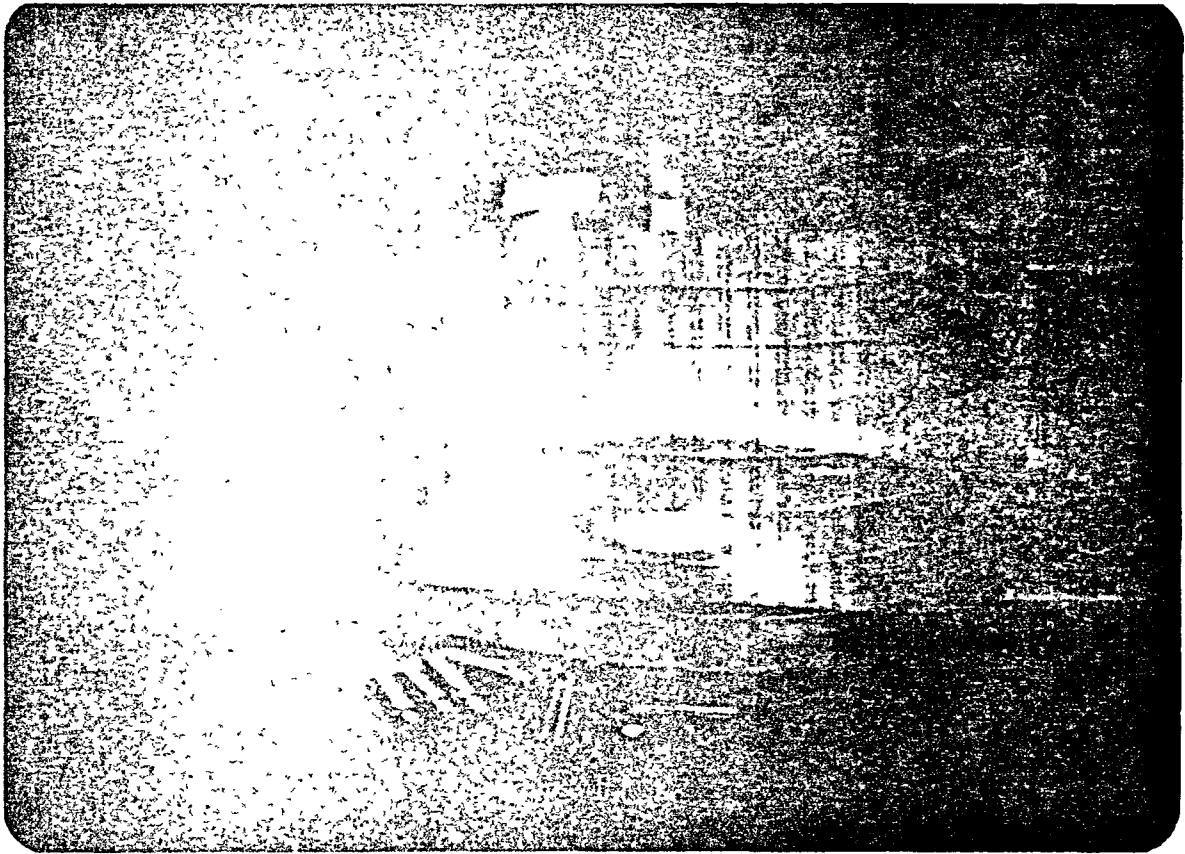


Figure 1. Experimental apparatus.

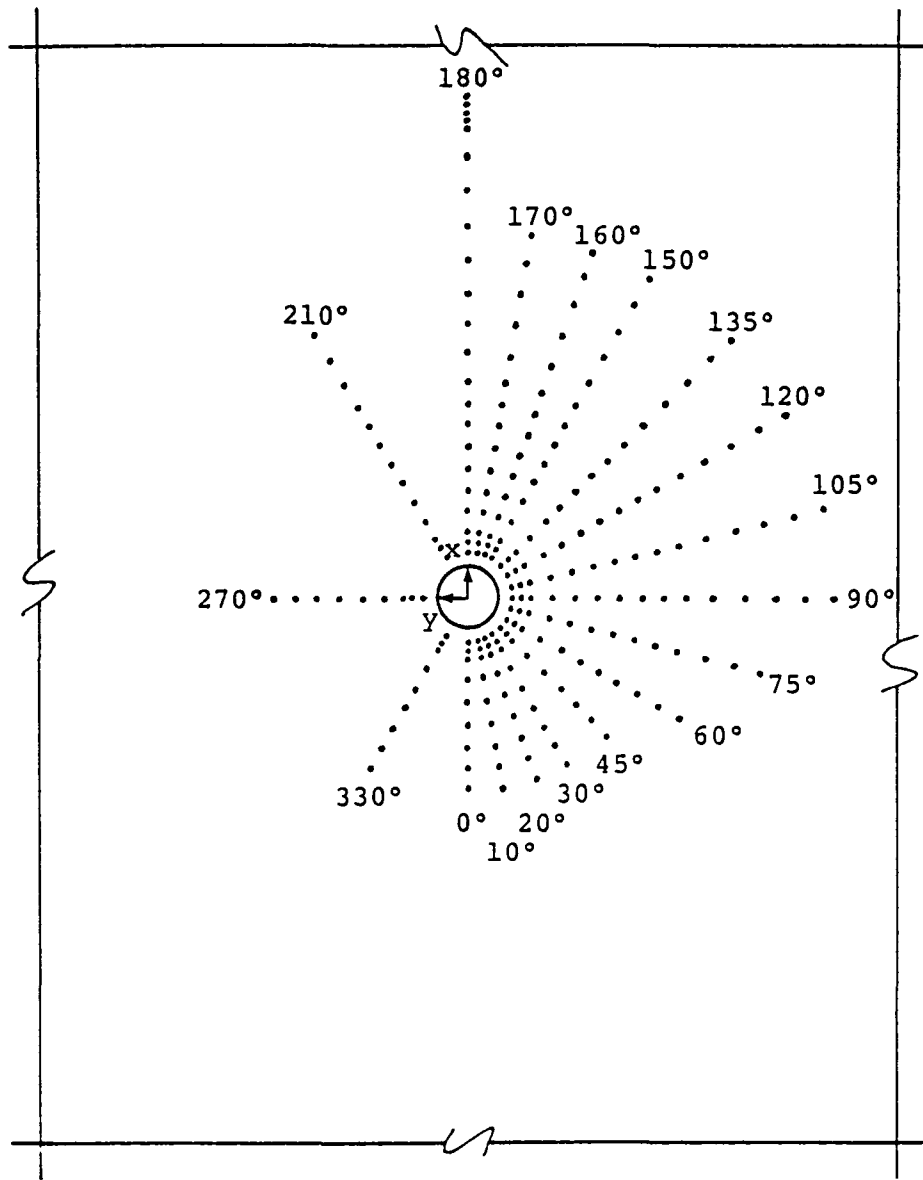


Figure 2. Flat plate pressure port distribution

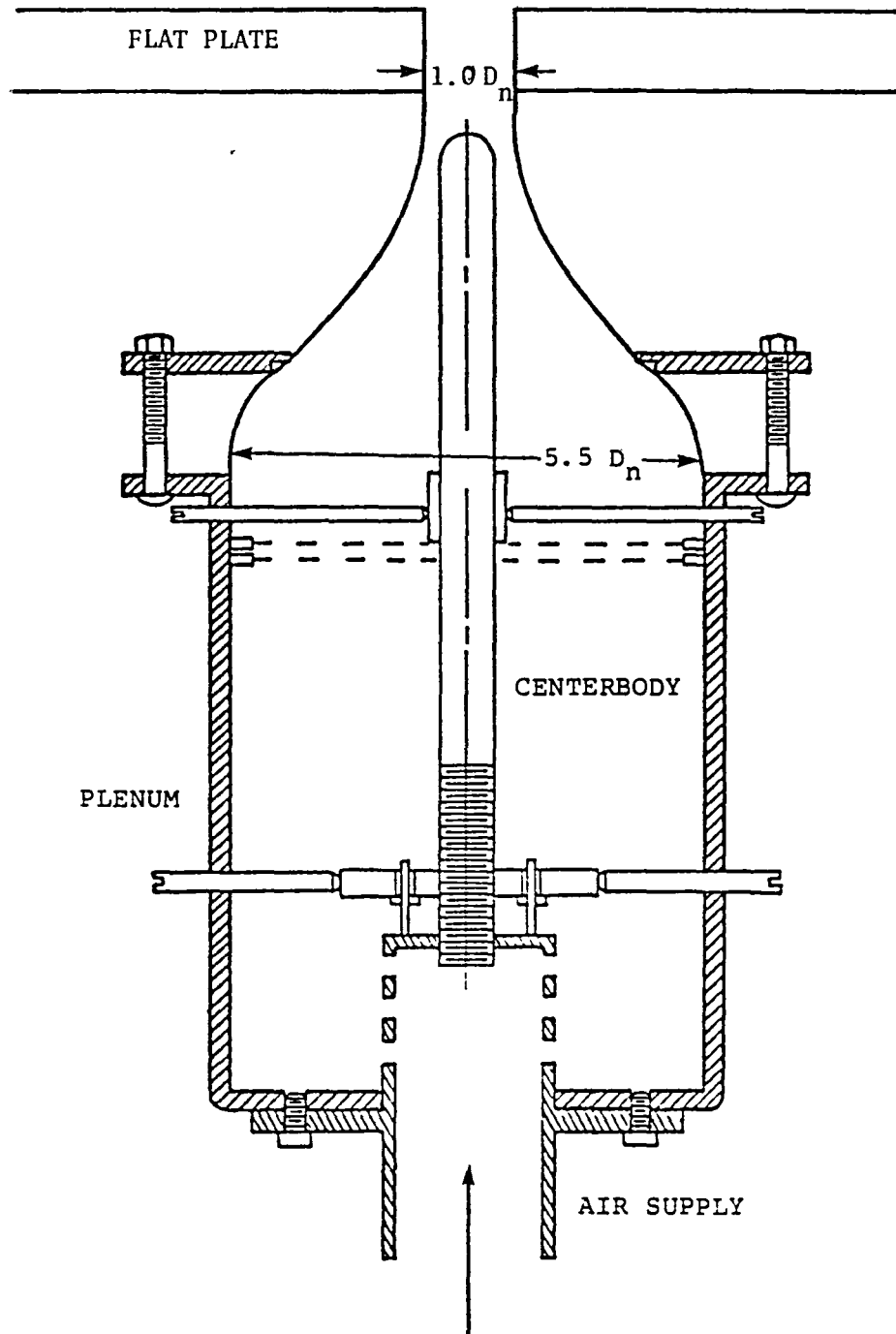


Figure 5. Cross section of jet nozzle, plenum and centerbody.



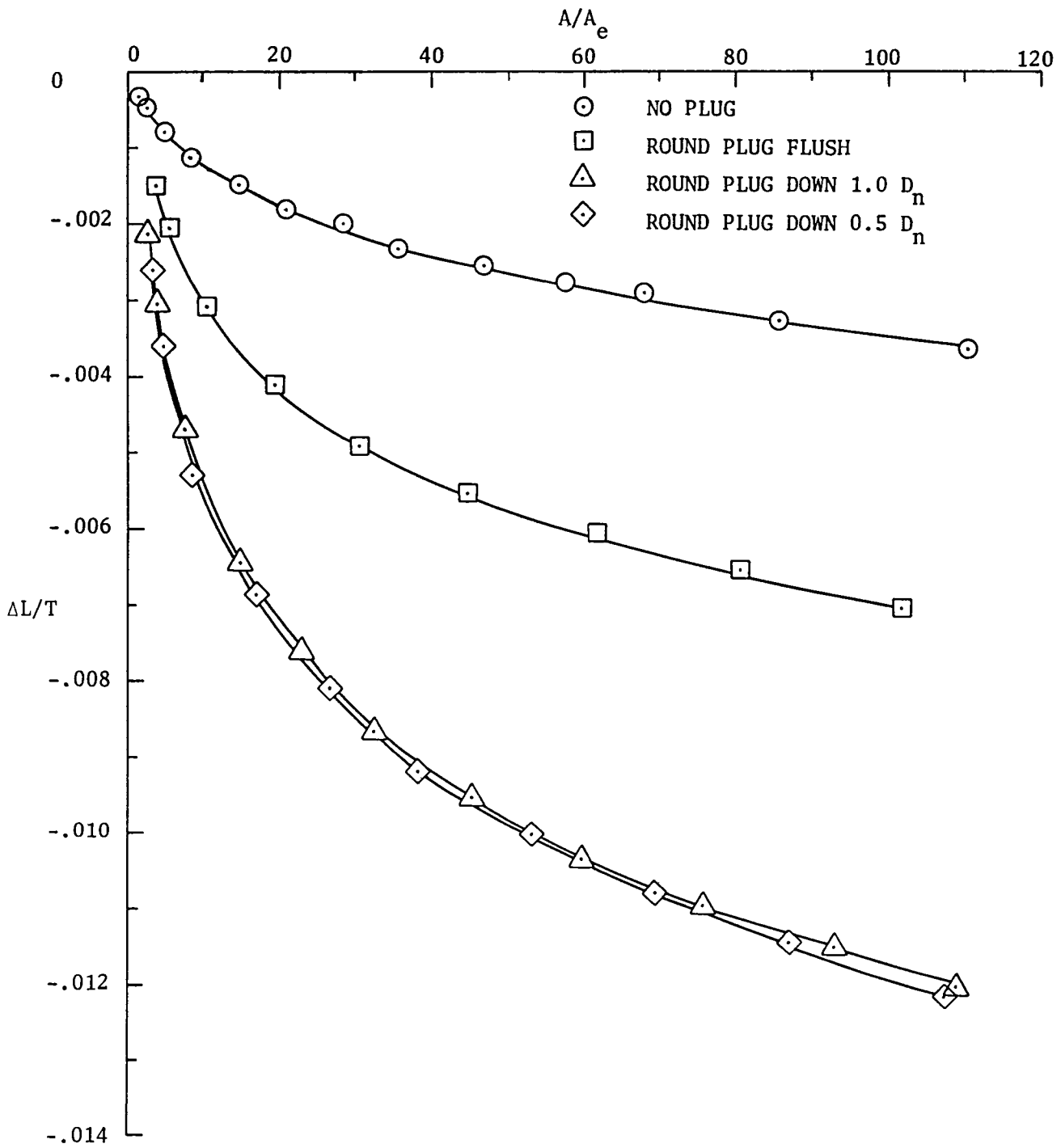


Figure 4. Nondimensional lift loss,  $\Delta L/T$ , for round-tipped plug configurations in hover compared with unplugged jet.

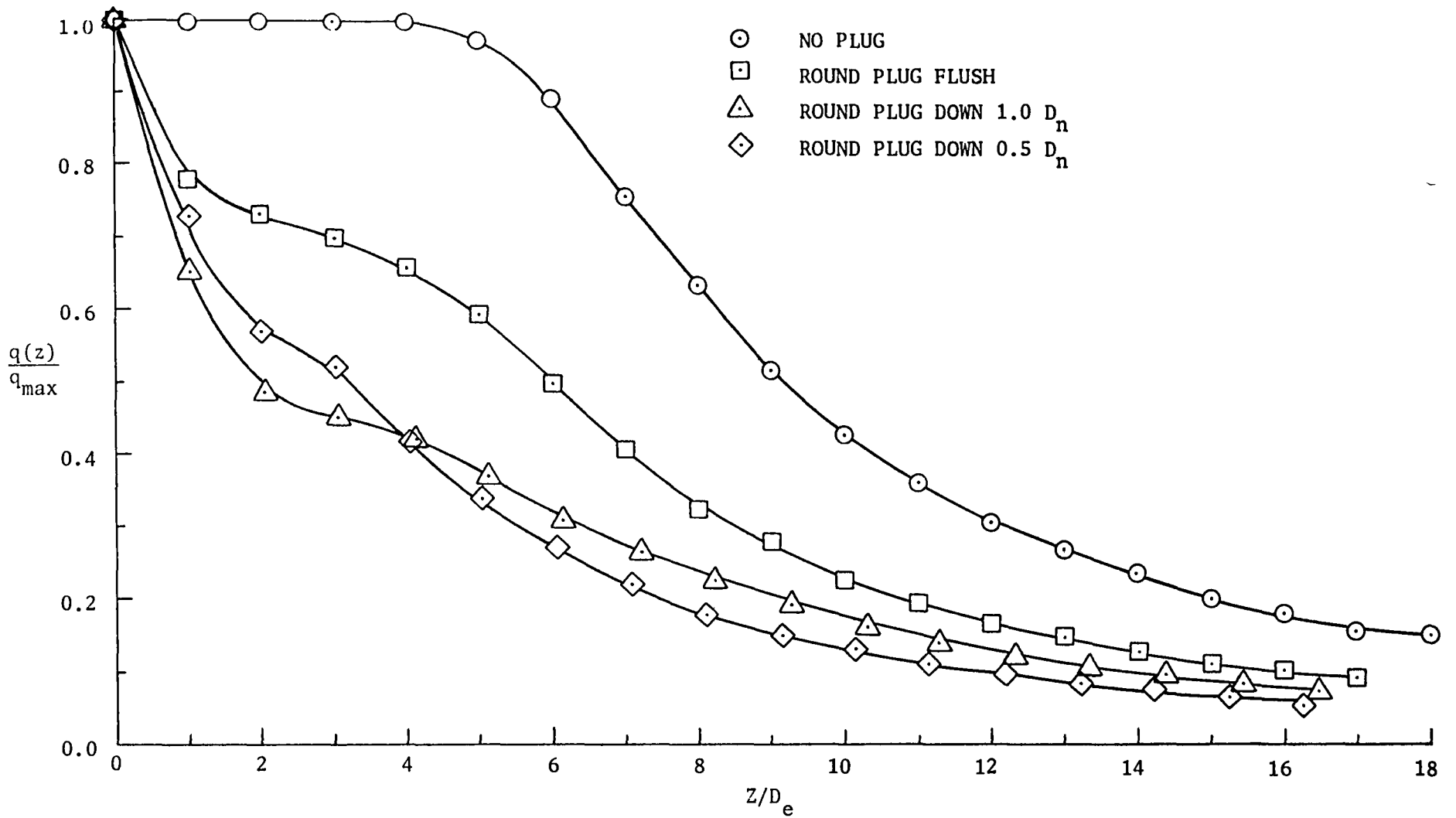


Figure 5. Jet centerline dynamic pressure decay for round-tipped plug configurations in hover compared with unplugged jet.

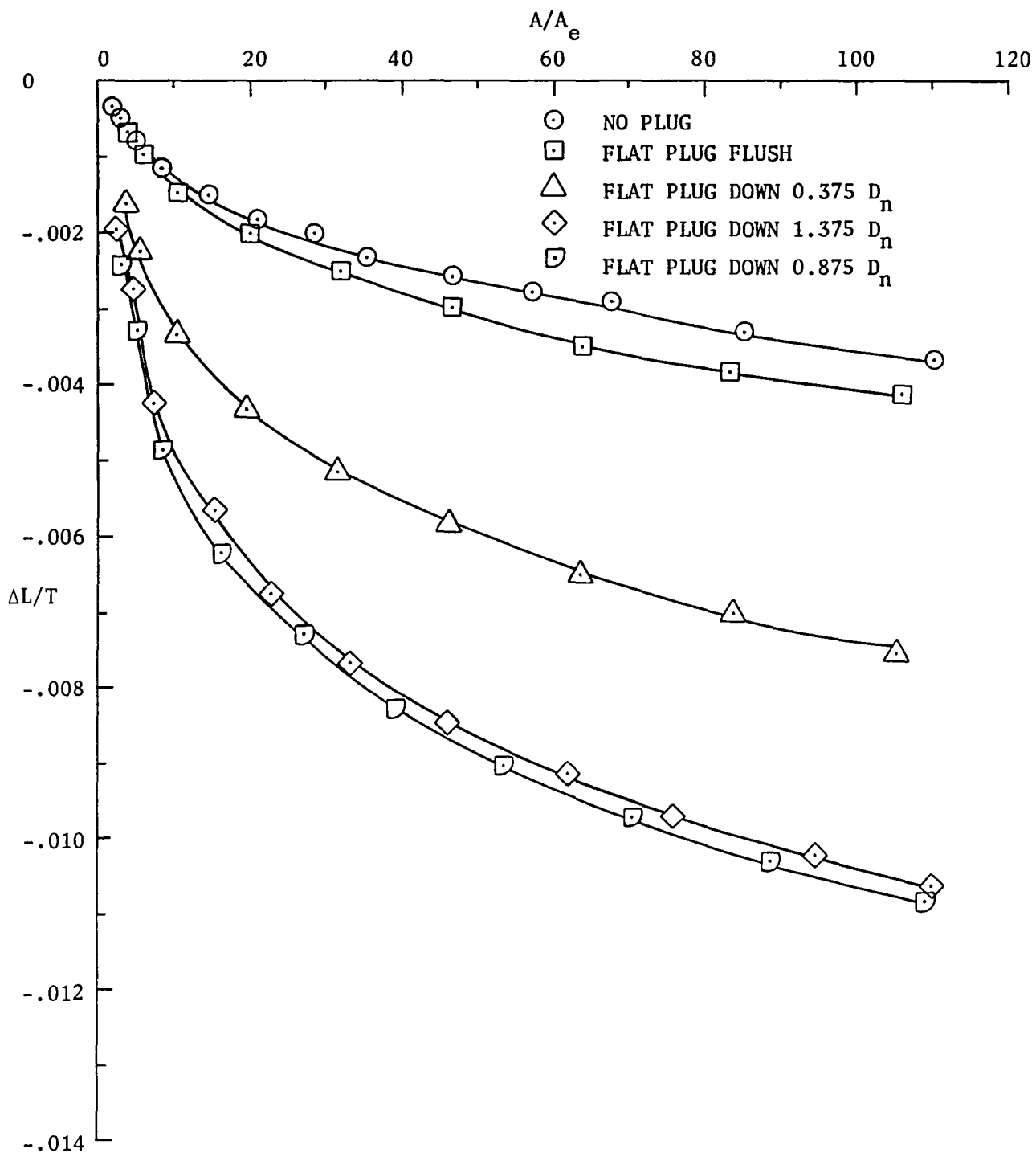


Figure 6. Nondimensional lift loss,  $\Delta L/T$ , for flat-tipped plug configurations in hover compared with unplugged jet.

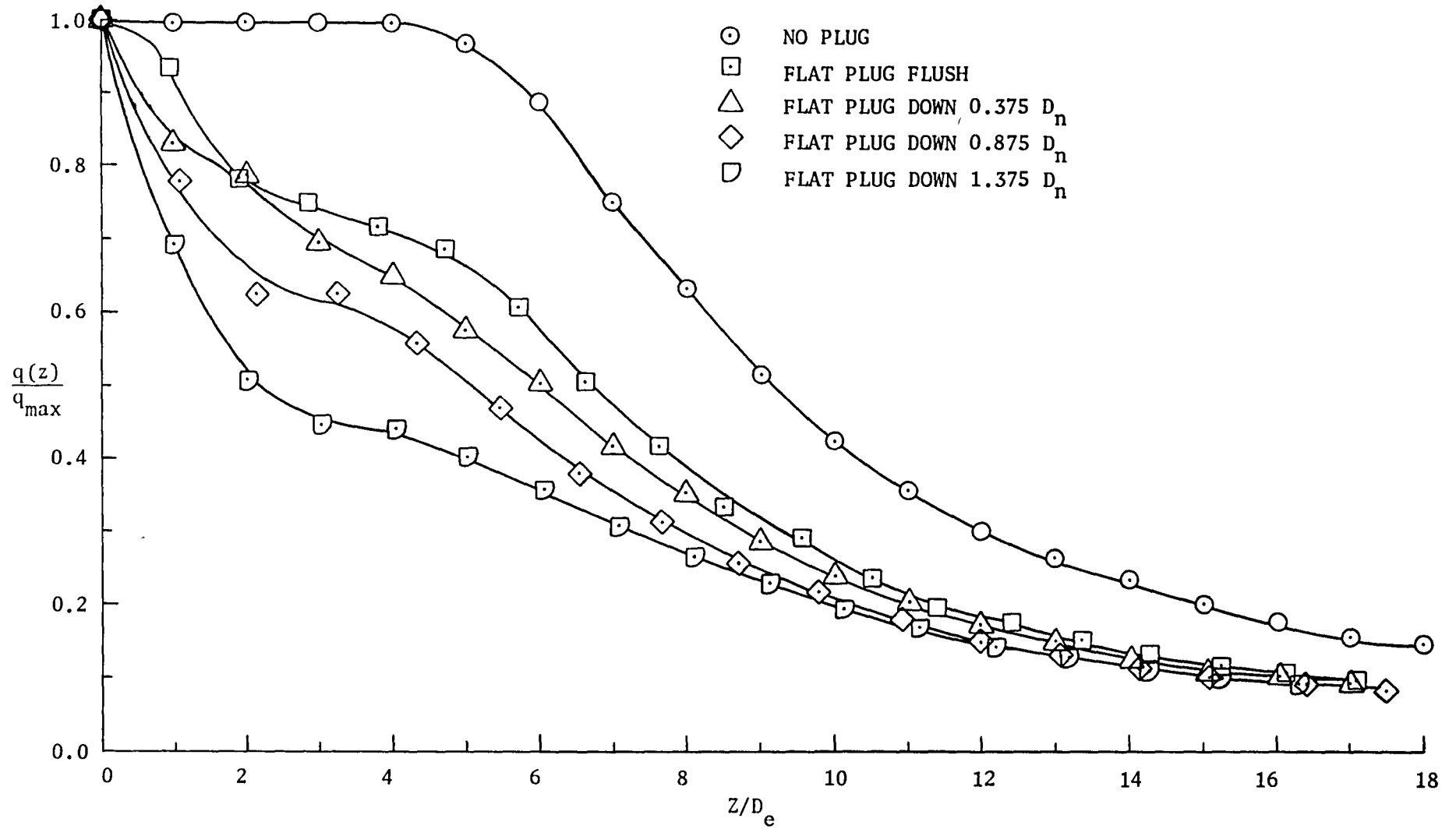


Figure 7. Jet centerline dynamic pressure decay for flat-tipped plug configurations in hover compared with unplugged jet.

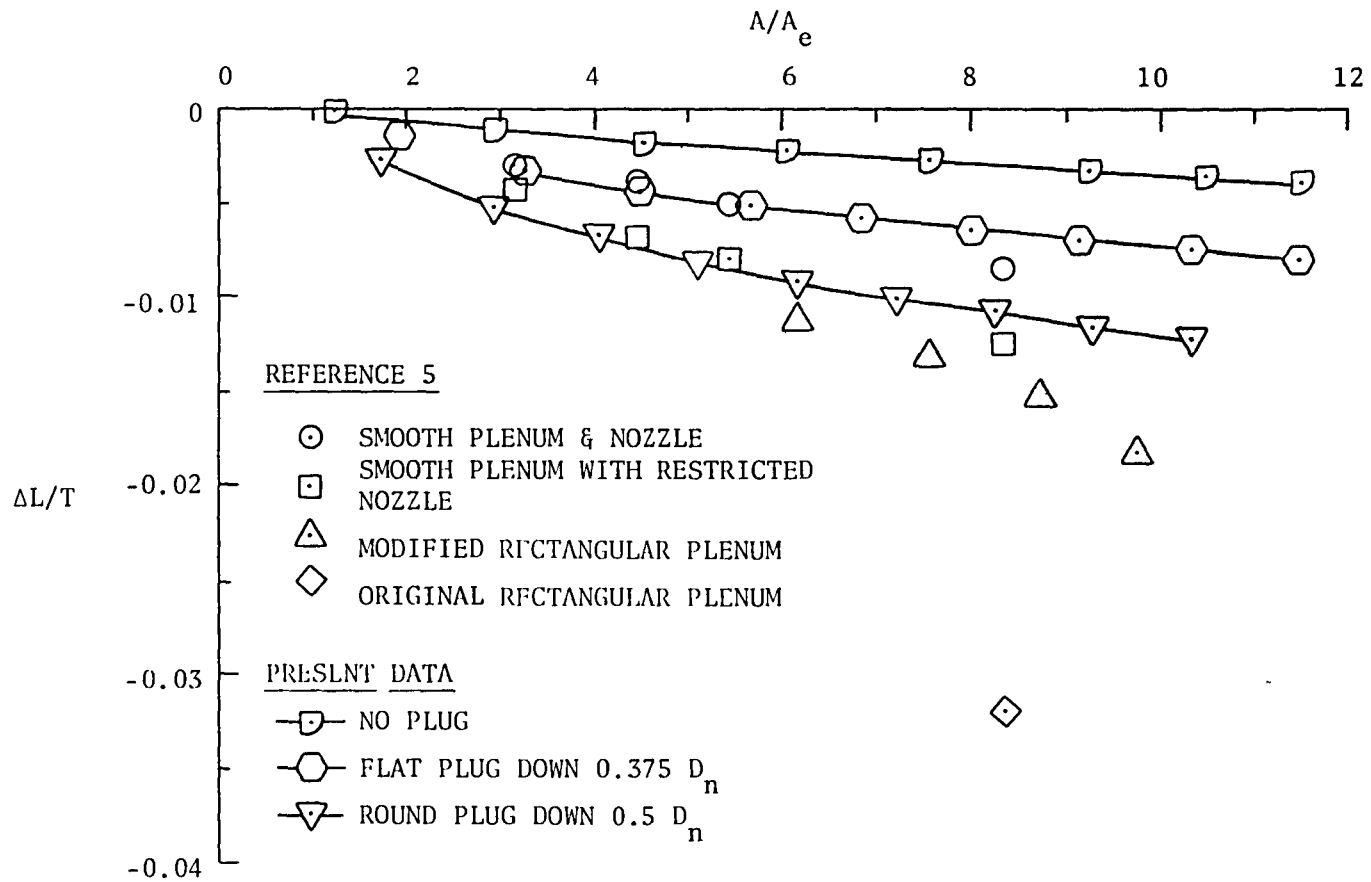


Figure 8. Comparison of induced lift loss for jet in hover with results of reference 5.

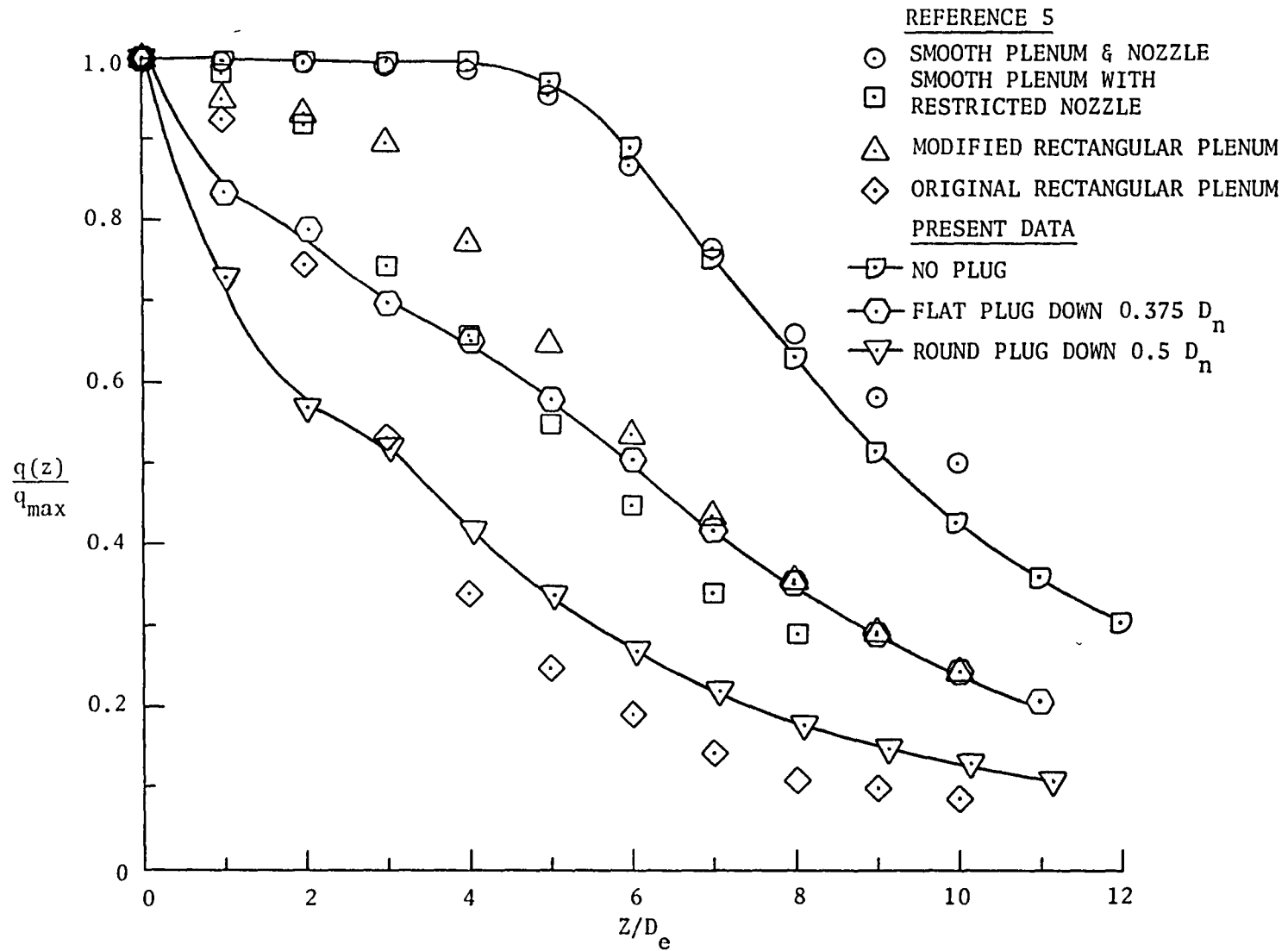


Figure 9. Comparison of dynamic pressure decay for jet in hover with results of reference 5.

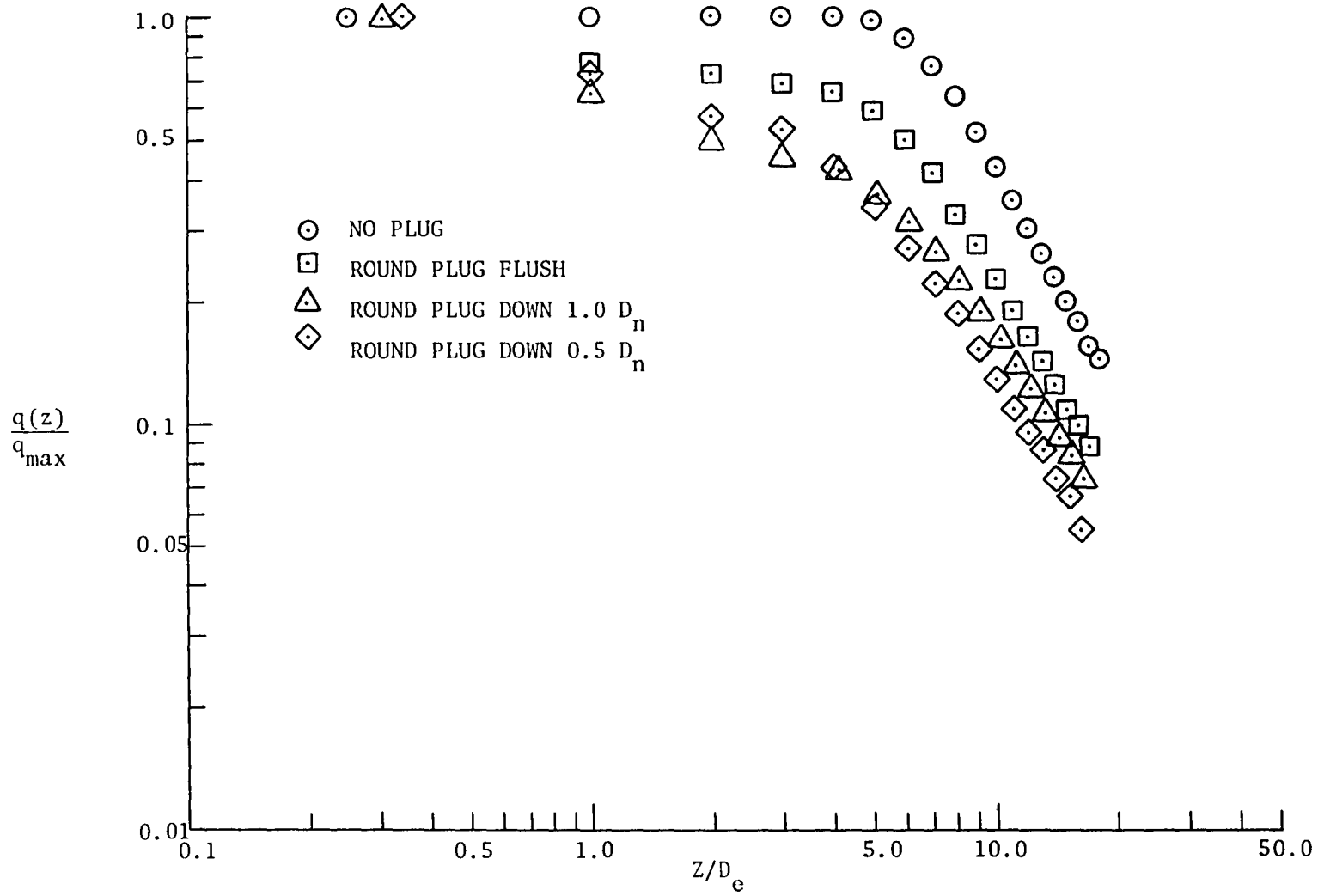


Figure 10. Logarithmic replot of hover jet dynamic pressure decay data; no plug and round plug configurations.

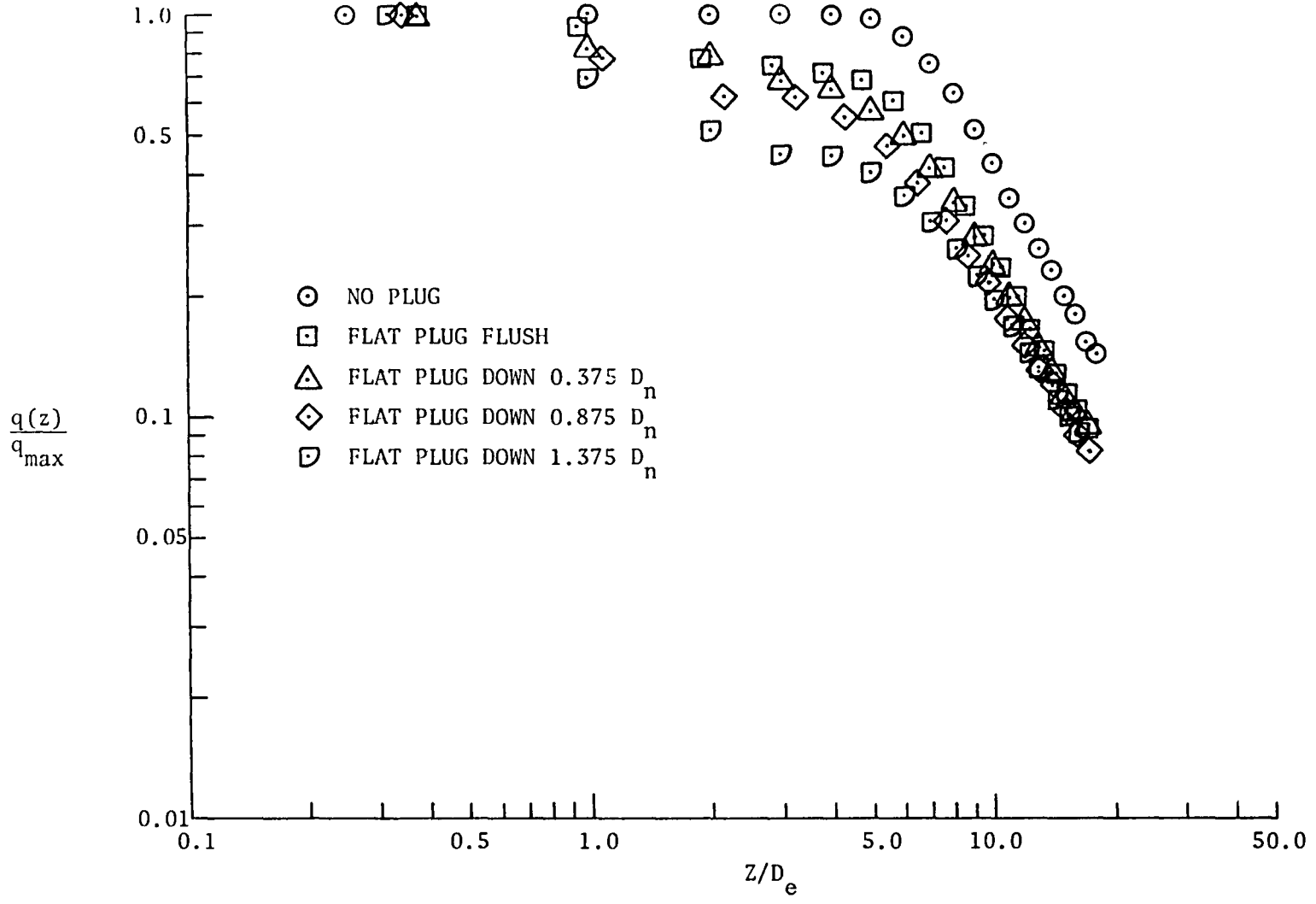


Figure 11. Logarithmic replot of hover jet dynamic pressure decay data; no plug and flat plug configurations.



APPENDIX A  
NOZZLE CALIBRATION DATA  
FOR JET IN HOVER

## APPENDIX A

### NOZZLE CALIBRATION DATA FOR JET IN HOVER

Nozzles used in the current work have been calibrated near the jet exit (at an elevation of 0.25 times the jet orifice diameter,  $D_n$ , above the exit plane) using the following procedure:

1. Record barometric pressure, nozzle exit pressure and exit temperature and jet flow rate.
2. Traverse  $0.25 D_n$  above nozzle exit plane across jet exit and record  $q$  versus  $r$ . Check for symmetry and adjust centerbody location if necessary.
3. Measure maximum observed jet exit dynamic pressure from  $q$  versus  $r$  from 2 above. (See figures A1-A7.)
4. Calculate jet thrust produced by equivalent ideal nozzle from the equation

$$T = \dot{m} \sqrt{\frac{2RT_e q_{\max}}{\left(P_e + \frac{\gamma - 1}{\gamma} q_{\max}\right)}}, \quad (A1)$$

where  $(P_e, T_e)$  are exit plane pressure and temperature,  $T$  is the calculated thrust,  $\dot{m}$  is the jet mass flow rate, and  $\gamma$  is the specific heat ratio.

5. Calculate effective jet exit plane velocity  $V_e$ , and effective jet area,  $A_e$ , and diameter,  $D_e$ , from

$$A_e = \frac{T}{2q_{\max}}, \quad (A2)$$

$$V_e = \frac{\dot{m}RT_e}{P_e A_e}, \quad (A3)$$

and

$$D_e = \sqrt{\frac{4A_e}{\pi}} . \quad (A4)$$

Nozzle exit plane total pressure and static pressure profiles are shown in figures A1 to A7. Dynamic pressures have been measured as total pressure minus static pressure. Nozzle calibration data are tabulated in table A1. Note that a  $q$  versus  $r$  profile has not been recorded for the round plug flush nozzle configuration. This was due to large unsteady fluctuations of  $q$ . To obtain a better measure of the maximum exit plane  $q$  for this configuration, the  $q$  values were electronically integrated at various  $r$  values, and the maximum observed average  $q$  has been recorded in table A1.

Table A1. Tabulated nozzle calibration for jet in hover.

Nozzle Calibration	Q m <sup>3</sup> /s (ft <sup>3</sup> /min)	T <sub>e</sub> K (R)	P <sub>e</sub> kPa (lb <sub>f</sub> /ft <sup>2</sup> )	q <sub>max</sub> kPa (lb <sub>f</sub> /ft <sup>2</sup> )	$\dot{m}$ kg/s (lb <sub>m</sub> /s)	T N (lb <sub>f</sub> )	D <sub>eff</sub> m (ft)	V <sub>eff</sub> m/s (ft/s)
No plug	0.0704 (149.1)	296 (533)	101.6 (2123)	11.52 (240.7)	0.0847 (0.1867)	11.57 (2.601)	0.0253 (0.083)	141 (463)
Round plug flush	0.0318 (67.43)	295 (531)	100.6 (2102)	11.30 (236.1)	0.0383 (0.0844)	5.20 (1.169)	0.0171 (0.0561)	140 (460)
Round plug 0.5 D <sub>n</sub> down	0.0378 (80.18)	296 (533)	102.4 (2138)	11.29 (235.8)	0.0455 (0.1004)	6.14 (1.3805)	0.0186 (0.061)	139 (456)
Round plug 1.0 D <sub>n</sub> down	0.0466 (98.75)	295 (531)	102.7 (2144)	12.78 (266.9)	0.0561 (0.1236)	8.00 (1.799)	0.0200 (0.0655)	148 (485)
Flat plug flush	0.0303 (64.13)	296 (533)	100.7 (2103)	11.13 (232.5)	0.0364 (0.0803)	4.92 (1.105)	0.0168 (0.055)	139 (457)
Flat plug 0.375 D <sub>n</sub> down	0.0314 (66.44)	296 (533)	102.5 (2140)	11.82 (246.8)	0.0377 (0.0832)	5.20 (1.169)	0.0167 (0.0549)	142 (467)
Flat plug 0.875 D <sub>n</sub> down	0.0360 (76.18)	295 (531)	101.5 (2120)	10.89 (227.5)	0.0433 (0.0954)	5.75 (1.292)	0.0183 (0.0601)	137 (449)
Flat plug 1.375 D <sub>n</sub> down	0.0443 (93.91)	296 (532)	101.2 (2113)	12.22 (255.2)	0.0533 (0.1176)	7.51 (1.688)	0.0198 (0.0649)	146 (478)

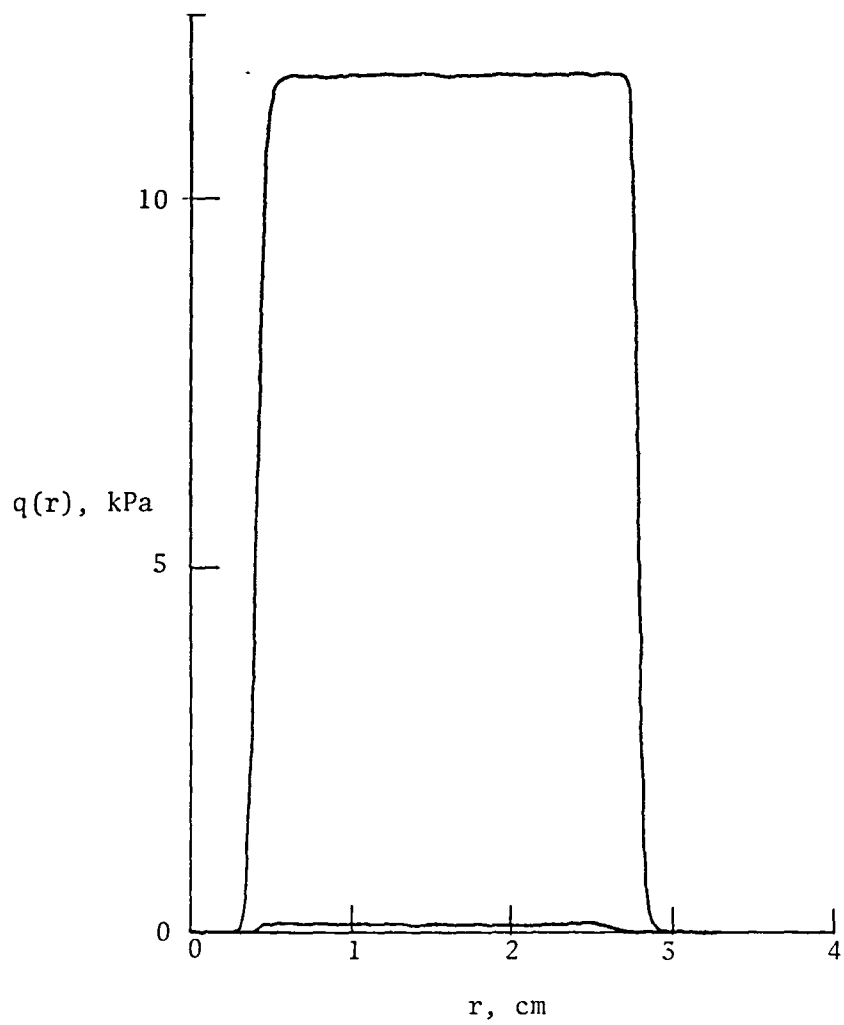


Figure A1. Nozzle exit plane dynamic pressure profile; no plug.

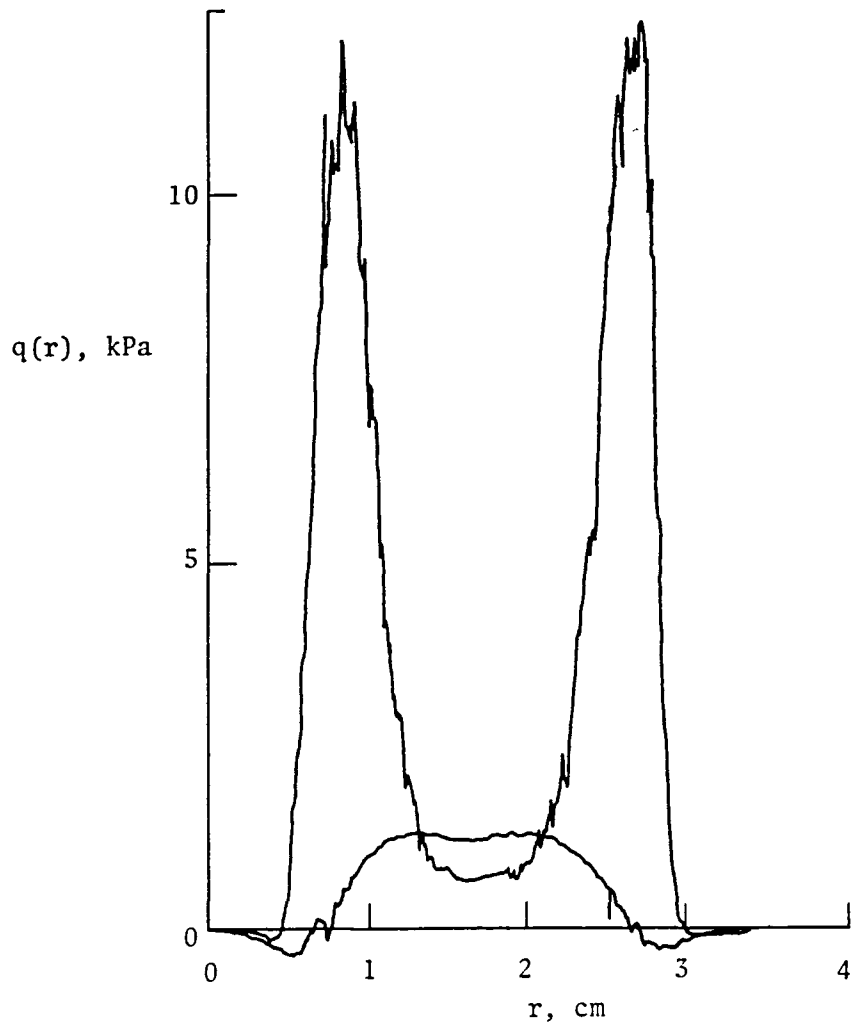


Figure A2. Nozzle exit plane dynamic pressure profile; round ended plug down  $0.5 D_n$ .

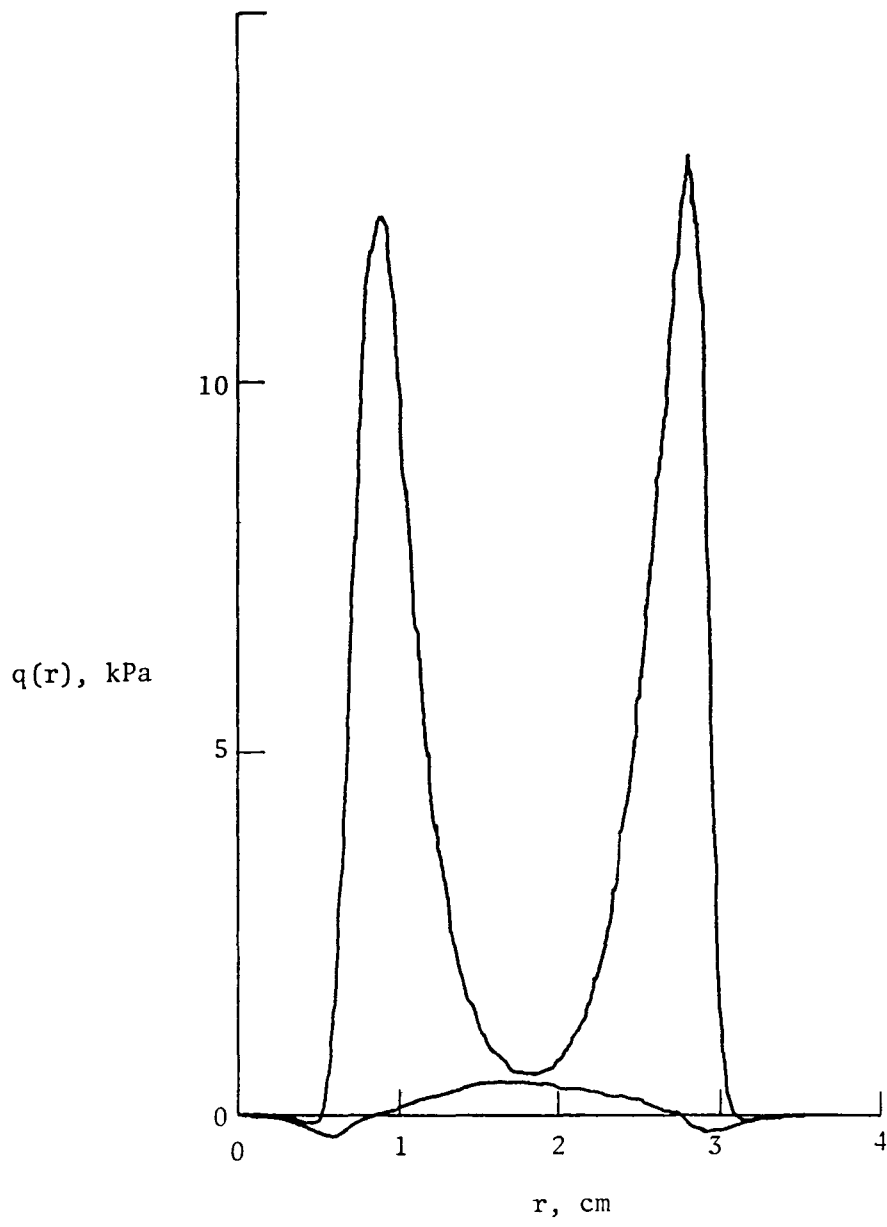


Figure A3. Nozzle exit plane dynamic pressure profile; round plug down  $1.0 D_n$ .

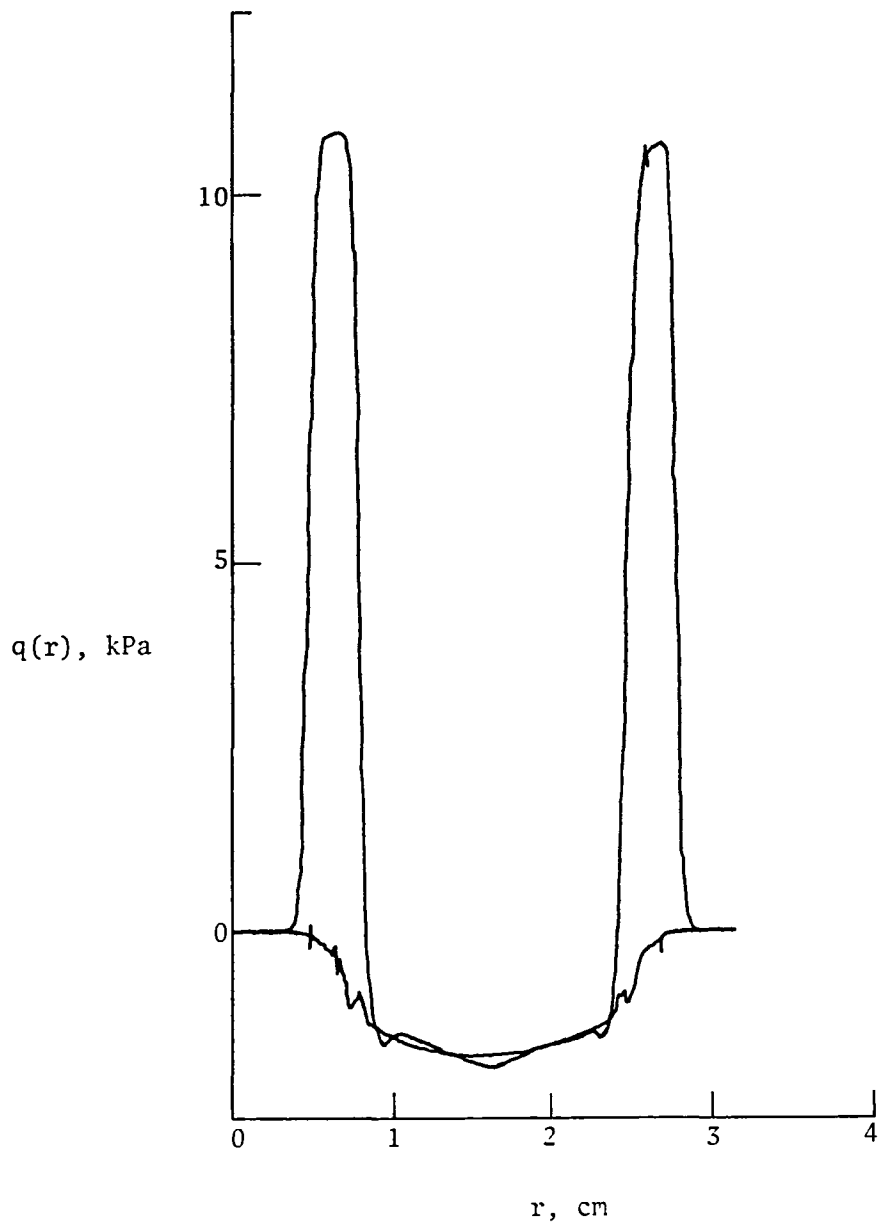


Figure A4. Nozzle exit plane dynamic pressure profile; flat plug flush.



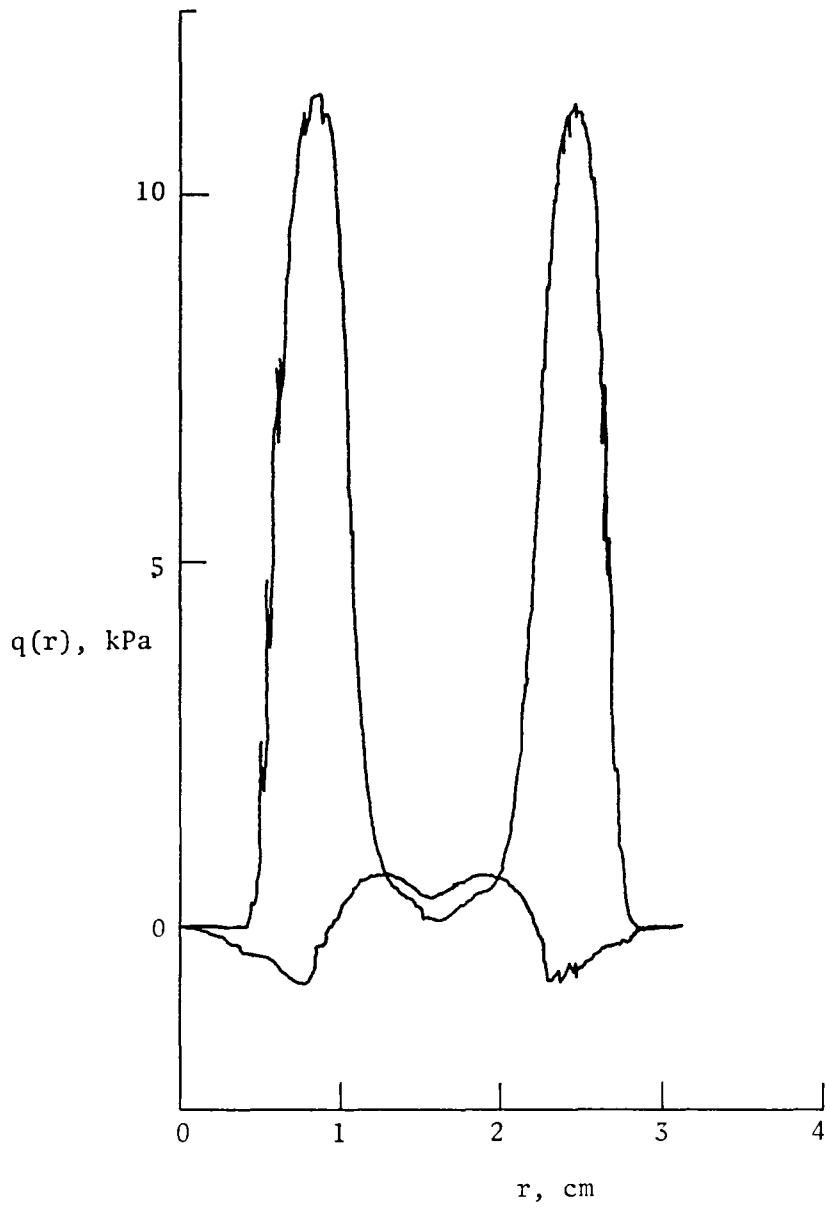


Figure A5. Nozzle exit plane dynamic pressure profile; flat plug down  $0.375 D_n$ .

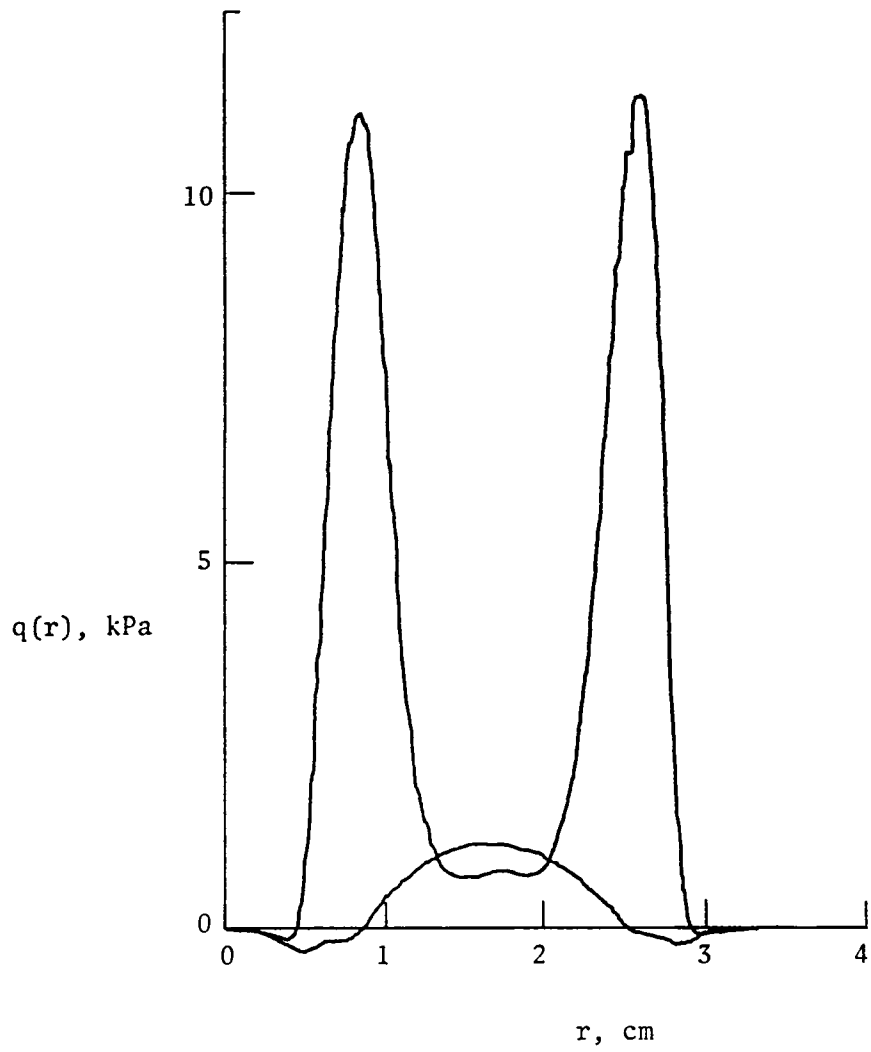


Figure A6. Nozzle exit plane dynamic pressure profile; flat plug down  $0.875 D_n$ .

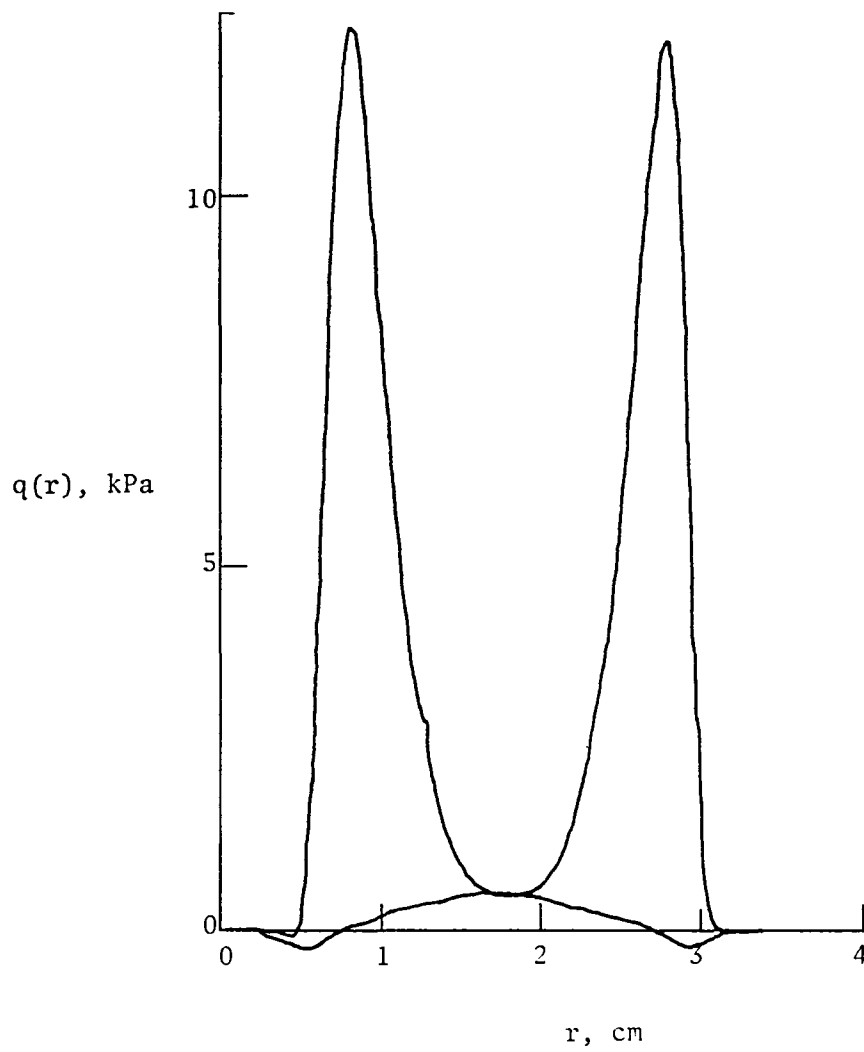


Figure A7. Nozzle exit plane dynamic pressure profile; flat plug down  $1.375 D_n$ .

APPENDIX B

TABULATED JET-IN-HOVER DYNAMIC  
PRESSURE DECAY DATA

Table B1. No plug.

---

$\frac{s}{D_{\text{eff}}}$	$\frac{q}{q_{\text{max}}}$
0.251	1.0
1	0.994
2	0.997
3	0.996
4	0.997
5	0.966
6	0.8831
7	0.753
8	0.633
9	0.518
10	0.426
11	0.357
12	0.304
13	0.262
14	0.23
15	0.199
16	0.18
17	0.153
18	0.143

---

Table B2. Round (hemispherical)-tipped plug flush.

---

$\frac{s}{D_{\text{eff}}}$	$\frac{q}{q_{\text{max}}}$
0	1.0
1	0.776
2	0.726
3	0.678 or 0.692
4	0.656
5	0.586
6	0.494
7	0.405
8	0.328
9	0.275
10	0.227
11	0.19
12	0.163
13	0.141
14	0.123
15	0.109
16	0.099
17	0.088

---

Table B3. Round (hemispherical)-tipped plug submerged  $0.5 D_n$ .

---

$\frac{s}{D_{\text{eff}}}$	$\frac{q}{q_{\text{max}}}$
0.341	1.0
1.017	0.729
2.033	0.571
3.05	0.524
4.066	0.422
5.083	0.34
6.099	0.273
7.116	0.22
8.132	0.187
9.149	0.153
10.165	0.131
11.182	0.108
12.199	0.096
13.215	0.086
14.232	0.073
15.248	0.066
16.265	0.054

---

Table B4. Round (hemispherical)-tipped plug submerged  $1.0 D_n$ .

$\frac{s}{D_{\text{eff}}}$	$\frac{q}{q_{\text{max}}}$
0.318	1.0
1.028	0.648
2.056	0.482
3.084	0.451
4.112	0.42
5.141	0.368
6.169	0.313
7.197	0.263
8.225	0.222
9.253	0.188
10.281	0.16
11.309	0.139
12.337	0.122
13.365	0.106
14.394	0.092
15.422	0.084
16.45	0.073



Table B5. Flat-tipped plug flush.

---

$\frac{s}{D_{\text{eff}}}$	$\frac{q}{q_{\text{max}}}$
0.379	1.0
0.952	0.934
1.903	0.78
2.86	0.743
3.806	0.713
4.758	0.688
5.709	0.607
6.661	0.502
7.612	0.419
8.564	0.336
9.515	0.283
10.467	0.233
11.418	0.2
12.37	0.168
13.321	0.149
14.273	0.129
15.224	0.114
16.176	0.104
17.127	0.093

---

Table B6. Flat-tipped plug submerged  $0.375 D_n$ .

---

$\frac{s}{D_{\text{eff}}}$	$\frac{q}{q_{\text{max}}}$
0.379	1.0
1.003	0.828
2.006	0.783
3.009	0.689
4.012	0.647
5.016	0.577
6.019	0.498
7.022	0.4135
8.025	0.345
9.028	0.284
10.031	0.239
11.034	0.202
12.037	0.176
13.04	0.151
14.043	0.131
15.047	0.118
16.05	0.106
17.053	0.097

---

Table B7. Flat-tipped plug submerged  $0.875 D_n$ .

---

$\frac{s}{D_{\text{eff}}}$	$\frac{q}{q_{\text{max}}}$
0.3466	1.0
1.092	0.777
2.184	0.623
3.276	0.627
4.368	0.556
5.46	0.467
6.552	0.38
7.644	0.316
8.736	0.256
9.829	0.219
10.92	0.179
12.01	0.153
13.105	0.133
14.197	0.122
15.289	0.105
16.381	0.091
17.473	0.082

---

Table B8. Flat-tipped plug submerged  $1.375 D_n$ .

---

$\frac{s}{D_{\text{eff}}}$	$\frac{q}{q_{\text{max}}}$
0.321	1.0
1.018	0.687
2.035	0.507
3.053	0.445
4.071	0.441
5.088	0.405
6.106	0.356
7.124	0.309
8.141	0.262
9.159	0.228
10.177	0.195
11.195	0.172
12.212	0.147
13.23	0.132
14.248	0.116
15.265	0.105
16.283	0.092

---

APPENDIX C

TABULATED STATIC PRESSURE DATA

FOR JET IN HOVER

Table C1. Flat plate pressure port locations.

Pressure Port No.	Radial Distance	
	cm	(in.)
1	1.905	(0.750)
2	2.223	(0.875)
3	2.540	(1.000)
4	3.493	(1.375)
5	4.445	(1.750)
6	5.398	(2.125)
7	6.350	(2.500)
8	7.303	(2.875)
9	8.255	(3.250)
10	9.208	(3.625)
11	10.160	(4.000)
12	11.430	(4.500)
13	12.700	(5.000)
14	13.970	(5.500)
15	15.240	(6.000)
16	16.510	(6.500)
17	17.780	(7.000)
18	19.050	(7.500)
19	20.320	(8.000)
20	20.638	(8.125)
21	20.955	(8.250)
22	21.273	(8.375)
23	21.590	(8.500)



PORT	NON-DIMENSIONAL	M	M	M/TD	L	L	LAT
	AREA						
1	1,6615	-0,000000	-0,000000	-0,000000	-0,003939	-0,000885	-0,000342
2	2,5476	-0,000000	-0,000000	-0,000000	-0,005677	-0,001276	-0,000492
3	4,6496	-0,000000	-0,000000	-0,000000	-0,009185	-0,002065	-0,000796
4	8,8770	-0,000000	-0,000000	-0,000000	-0,013386	-0,003009	-0,001161
5	13,1936	-0,000000	-0,000000	-0,000000	-0,017169	-0,003860	-0,001489
6	20,6496	-0,000000	-0,000000	-0,000000	-0,020600	-0,004631	-0,001786
7	28,2449	-0,000000	-0,000000	-0,000000	-0,023815	-0,005354	-0,002065
8	36,9794	-0,000000	-0,000000	-0,000000	-0,026615	-0,005983	-0,002308
9	46,8532	-0,000000	-0,000000	-0,000000	-0,029508	-0,006633	-0,002559
10	57,8663	-0,000000	-0,000000	-0,000000	-0,032146	-0,007226	-0,002787
11	67,9142	-0,000000	-0,000000	-0,000000	-0,034188	-0,007686	-0,002965
12	85,6365	-0,000000	-0,000000	-0,000000	-0,037738	-0,008483	-0,003272
13	110,6375	-0,000000	-0,000000	-0,000000	-0,042172	-0,009480	-0,003657
14	132,9169	-0,000000	-0,000000	-0,000000	-0,045593	-0,010249	-0,003954
15	157,2218	-0,000000	-0,000000	-0,000000	-0,048879	-0,010988	-0,004238
16	183,5520	-0,000000	-0,000000	-0,000000	-0,051504	-0,011578	-0,004466
17	211,9076	-0,000000	-0,000000	-0,000000	-0,054595	-0,012273	-0,004734
18	242,2886	-0,000000	-0,000000	-0,000000	-0,057131	-0,012843	-0,004954
19	262,3053	-0,000000	-0,000000	-0,000000	-0,058478	-0,013146	-0,005071
20	270,5334	-0,000000	-0,000000	-0,000000	-0,059383	-0,013349	-0,005149
21	278,8882	-0,000000	-0,000000	-0,000000	-0,059917	-0,013469	-0,005196
22	287,3696	-0,000000	-0,000000	-0,000000	-0,060791	-0,013666	-0,005271
23	295,9775	-0,000000	-0,000000	-0,000000	-0,061261	-0,013771	-0,005312





PORT	NON-DIMENSIONAL AREA	M		M/TD	L		L/T
		N -M	LB-FT		N	LB	
1	2,6532	-0.000000	-0.000000	-0.000000	-0.017311	-0.003092	-0.002162
2	4,0683	-0.000000	-0.000000	-0.000000	-0.024461	-0.005499	-0.003054
3	7,5049	-0.000000	-0.000000	-0.000000	-0.037777	-0.008492	-0.004717
4	14,1759	-0.000000	-0.000000	-0.000000	-0.050944	-0.011452	-0.006361
5	22,6662	-0.000000	-0.000000	-0.000000	-0.060968	-0.013706	-0.007612
6	32,9760	-0.000000	-0.000000	-0.000000	-0.069453	-0.015613	-0.008672
7	45,1050	-0.000000	-0.000000	-0.000000	-0.076617	-0.017224	-0.009566
8	59,0535	-0.000000	-0.000000	-0.000000	-0.082842	-0.018623	-0.010344
9	74,8213	-0.000000	-0.000000	-0.000000	-0.087908	-0.019762	-0.010976
10	92,4005	-0.000000	-0.000000	-0.000000	-0.092690	-0.020837	-0.011573
11	108,4543	-0.000000	-0.000000	-0.000000	-0.096245	-0.021636	-0.012017
12	136,7555	-0.000000	-0.000000	-0.000000	-0.101175	-0.022744	-0.012633
13	176,6004	-0.000000	-0.000000	-0.000000	-0.107157	-0.024089	-0.013300
14	212,7590	-0.000000	-0.000000	-0.000000	-0.112093	-0.025198	-0.013996
15	251,0721	-0.000000	-0.000000	-0.000000	-0.116929	-0.026286	-0.014600
16	293,1196	-0.000000	-0.000000	-0.000000	-0.121371	-0.027284	-0.015154
17	338,4015	-0.000000	-0.000000	-0.000000	-0.125508	-0.028214	-0.015671
18	386,9179	-0.000000	-0.000000	-0.000000	-0.129660	-0.029148	-0.016189
19	418,8831	-0.000000	-0.000000	-0.000000	-0.131990	-0.029671	-0.016480
20	432,0729	-0.000000	-0.000000	-0.000000	-0.133045	-0.029909	-0.016612
21	445,3649	-0.000000	-0.000000	-0.000000	-0.133862	-0.030092	-0.016714
22	458,9091	-0.000000	-0.000000	-0.000000	-0.134785	-0.030300	-0.016829
23	472,6551	-0.000000	-0.000000	-0.000000	-0.135432	-0.030445	-0.016910



PORT	NON-DIMENSIONAL AREA	N -M	M Lb-ft	M/TD	N	L Lb	L/T
1	2.7465	-0.000000	-0.000000	-0.000000	-0.014632	-0.003289	-0.001949
2	4.1500	-0.000000	-0.000000	-0.000000	-0.020668	-0.004646	-0.002753
3	7.6555	-0.000000	-0.000000	-0.000000	-0.031784	-0.007145	-0.004233
4	14.4604	-0.000000	-0.000000	-0.000000	-0.042600	-0.009576	-0.005674
5	23.1212	-0.000000	-0.000000	-0.000000	-0.050680	-0.011393	-0.006750
6	33.6379	-0.000000	-0.000000	-0.000000	-0.057565	-0.012941	-0.007667
7	46.0105	-0.000000	-0.000000	-0.000000	-0.063508	-0.014277	-0.008459
8	60.2389	-0.000000	-0.000000	-0.000000	-0.068527	-0.015405	-0.009127
9	76.3233	-0.000000	-0.000000	-0.000000	-0.072838	-0.016374	-0.009701
10	94.2635	-0.000000	-0.000000	-0.000000	-0.076731	-0.017249	-0.010220
11	110.6313	-0.000000	-0.000000	-0.000000	-0.079791	-0.017937	-0.010627
12	139.5007	-0.000000	-0.000000	-0.000000	-0.083701	-0.018816	-0.011148
13	180.2270	-0.000000	-0.000000	-0.000000	-0.088345	-0.019860	-0.011767
14	216.5199	-0.000000	-0.000000	-0.000000	-0.091892	-0.020657	-0.012239
15	256.1121	-0.000000	-0.000000	-0.000000	-0.095280	-0.021419	-0.012690
16	299.0036	-0.000000	-0.000000	-0.000000	-0.098309	-0.022100	-0.013094
17	345.1945	-0.000000	-0.000000	-0.000000	-0.101402	-0.022795	-0.013506
18	394.6848	-0.000000	-0.000000	-0.000000	-0.104378	-0.023464	-0.013902
19	427.2917	-0.000000	-0.000000	-0.000000	-0.106272	-0.023890	-0.014154
20	440.6953	-0.000000	-0.000000	-0.000000	-0.106987	-0.024051	-0.014250
21	454.3051	-0.000000	-0.000000	-0.000000	-0.107663	-0.024203	-0.014340
22	468.1211	-0.000000	-0.000000	-0.000000	-0.108256	-0.024336	-0.014419
23	482.1434	-0.000000	-0.000000	-0.000000	-0.109011	-0.024506	-0.014519



PORT	NON-DIMENSIONAL AREA	N - M	M LB-FT	M/TD	N	L LB	L/T
1	3,0575	-0,000000	-0,000000	-0,000000	-0,015794	-0,003550	-0,002572
2	4,6002	-0,000000	-0,000000	-0,000000	-0,021790	-0,004898	-0,003548
3	8,6404	-0,000000	-0,000000	-0,000000	-0,032431	-0,007291	-0,005281
4	16,3360	-0,000000	-0,000000	-0,000000	-0,042081	-0,009460	-0,006853
5	26,1201	-0,000000	-0,000000	-0,000000	-0,049799	-0,011195	-0,008109
6	38,0008	-0,000000	-0,000000	-0,000000	-0,056131	-0,012618	-0,009141
7	51,9700	-0,000000	-0,000000	-0,000000	-0,061346	-0,013791	-0,009990
8	68,0519	-0,000000	-0,000000	-0,000000	-0,066078	-0,014854	-0,010760
9	86,2224	-0,000000	-0,000000	-0,000000	-0,070288	-0,015801	-0,011446
10	106,4895	-0,000000	-0,000000	-0,000000	-0,074458	-0,016738	-0,012125
11	124,9803	-0,000000	-0,000000	-0,000000	-0,077523	-0,017427	-0,012624
12	157,5939	-0,000000	-0,000000	-0,000000	-0,081950	-0,018422	-0,013345
13	203,6025	-0,000000	-0,000000	-0,000000	-0,087074	-0,019574	-0,014180
14	244,6026	-0,000000	-0,000000	-0,000000	-0,090711	-0,020392	-0,014772
15	289,3299	-0,000000	-0,000000	-0,000000	-0,094210	-0,021178	-0,015342
16	337,7845	-0,000000	-0,000000	-0,000000	-0,097673	-0,021957	-0,015906
17	389,9661	-0,000000	-0,000000	-0,000000	-0,100555	-0,022605	-0,016375
18	445,8755	-0,000000	-0,000000	-0,000000	-0,102734	-0,023095	-0,016730
19	482,7115	-0,000000	-0,000000	-0,000000	-0,104443	-0,023479	-0,017008
20	497,8536	-0,000000	-0,000000	-0,000000	-0,105321	-0,023676	-0,017151
21	513,2206	-0,000000	-0,000000	-0,000000	-0,106092	-0,023849	-0,017277
22	528,8366	-0,000000	-0,000000	-0,000000	-0,106664	-0,023978	-0,017370
23	544,6775	-0,000000	-0,000000	-0,000000	-0,107289	-0,024119	-0,017471



PORT	NON-DIMENSIONAL APFA	M		M/TD	L		L/T
		N -M	LB-FT		N	LB	
1	3.1526	-0.000000	-0.000000	-0.000000	-0.013701	-0.003080	-0.002385
2	4.8340	-0.000000	-0.000000	-0.000000	-0.018739	-0.004213	-0.003261
3	8.9174	-0.000000	-0.000000	-0.000000	-0.027712	-0.006230	-0.004823
4	16.8440	-0.000000	-0.000000	-0.000000	-0.035665	-0.008818	-0.006207
5	26.9324	-0.000000	-0.000000	-0.000000	-0.041907	-0.009421	-0.007294
6	39.1826	-0.000000	-0.000000	-0.000000	-0.047243	-0.010670	-0.008222
7	53.5947	-0.000000	-0.000000	-0.000000	-0.051783	-0.011641	-0.009012
8	70.1685	-0.000000	-0.000000	-0.000000	-0.055736	-0.012530	-0.009700
9	88.9041	-0.000000	-0.000000	-0.000000	-0.059391	-0.013351	-0.010336
10	109.8015	-0.000000	-0.000000	-0.000000	-0.062502	-0.014050	-0.010878
11	128.8674	-0.000000	-0.000000	-0.000000	-0.064809	-0.014569	-0.011279
12	162.4954	-0.000000	-0.000000	-0.000000	-0.068537	-0.015407	-0.011928
13	209.9349	-0.000000	-0.000000	-0.000000	-0.072785	-0.016362	-0.012668
14	252.2101	-0.000000	-0.000000	-0.000000	-0.075597	-0.016994	-0.013157
15	298.3285	-0.000000	-0.000000	-0.000000	-0.078059	-0.017548	-0.013585
16	348.2902	-0.000000	-0.000000	-0.000000	-0.080840	-0.018173	-0.014070
17	402.0950	-0.000000	-0.000000	-0.000000	-0.083959	-0.018874	-0.014612
18	459.7430	-0.000000	-0.000000	-0.000000	-0.084429	-0.018980	-0.014694
19	497.7247	-0.000000	-0.000000	-0.000000	-0.085358	-0.019188	-0.014856
20	513.3377	-0.000000	-0.000000	-0.000000	-0.086065	-0.019347	-0.014979
21	529.1909	-0.000000	-0.000000	-0.000000	-0.086553	-0.019457	-0.015064
22	545.2843	-0.000000	-0.000000	-0.000000	-0.087242	-0.019621	-0.015191
23	561.6179	-0.000000	-0.000000	-0.000000	-0.088169	-0.019821	-0.015345





PORT	NON-DIMENSIONAL AREA	N - M	M LB-FT	M/TD	N	L LB	L/T
1	3,6146	-0.000000	-0.000000	-0.000000	-0.007635	-0.001716	-0.001469
2	5,5424	-0.000000	-0.000000	-0.000000	-0.010645	-0.002393	-0.002047
3	10,2741	-0.000000	-0.000000	-0.000000	-0.016116	-0.003623	-0.003100
4	19,3122	-0.000000	-0.000000	-0.000000	-0.021429	-0.004817	-0.004122
5	30,8789	-0.000000	-0.000000	-0.000000	-0.025538	-0.005741	-0.004912
6	44,9242	-0.000000	-0.000000	-0.000000	-0.028853	-0.006486	-0.005550
7	61,4480	-0.000000	-0.000000	-0.000000	-0.031690	-0.007124	-0.006095
8	80,4504	-0.000000	-0.000000	-0.000000	-0.034279	-0.007706	-0.006593
9	101,9314	-0.000000	-0.000000	-0.000000	-0.036659	-0.008241	-0.007051
10	125,8910	-0.000000	-0.000000	-0.000000	-0.038789	-0.008720	-0.007461
11	147,7507	-0.000000	-0.000000	-0.000000	-0.040425	-0.009088	-0.007775
12	186,3063	-0.000000	-0.000000	-0.000000	-0.042950	-0.009655	-0.008261
13	240,6972	-0.000000	-0.000000	-0.000000	-0.046061	-0.010355	-0.008859
14	289,1672	-0.000000	-0.000000	-0.000000	-0.048159	-0.010826	-0.009263
15	342,0434	-0.000000	-0.000000	-0.000000	-0.050331	-0.011314	-0.009681
16	399,3261	-0.000000	-0.000000	-0.000000	-0.052790	-0.011867	-0.010154
17	461,0151	-0.000000	-0.000000	-0.000000	-0.054716	-0.012300	-0.010524
18	527,1104	-0.000000	-0.000000	-0.000000	-0.056857	-0.012782	-0.010936
19	570,6576	-0.000000	-0.000000	-0.000000	-0.057792	-0.012992	-0.011116
20	588,5585	-0.000000	-0.000000	-0.000000	-0.058149	-0.013072	-0.011184
21	606,7347	-0.000000	-0.000000	-0.000000	-0.058532	-0.013158	-0.011258
22	625,1863	-0.000000	-0.000000	-0.000000	-0.058805	-0.013219	-0.011311
23	643,9133	-0.000000	-0.000000	-0.000000	-0.059258	-0.013321	-0.011398



5

PORT	NON-DIMENSIONAL AREA	N - M	M LB-FT	M/TD	N	L LB	L/T
1	3,7786	-0.000000	-0.000000	-0.000000	-0.0008583	-0.001930	-0.001651
2	5,7934	-0.000000	-0.000000	-0.000000	-0.011746	-0.002640	-0.002259
3	10,6884	-0.000000	-0.000000	-0.000000	-0.017316	-0.003893	-0.003330
4	20,1885	-0.000000	-0.000000	-0.000000	-0.022452	-0.005047	-0.004318
5	32,2799	-0.000000	-0.000000	-0.000000	-0.026756	-0.006015	-0.005146
6	46,9625	-0.000000	-0.000000	-0.000000	-0.030272	-0.006805	-0.005822
7	64,2364	-0.000000	-0.000000	-0.000000	-0.033444	-0.007518	-0.006432
8	84,1406	-0.000000	-0.000000	-0.000000	-0.036160	-0.008129	-0.006954
9	106,5562	-0.000000	-0.000000	-0.000000	-0.038878	-0.008740	-0.007477
10	131,6028	-0.000000	-0.000000	-0.000000	-0.040985	-0.009214	-0.007883
11	154,4543	-0.000000	-0.000000	-0.000000	-0.042575	-0.009571	-0.008188
12	194,7593	-0.000000	-0.000000	-0.000000	-0.044957	-0.010106	-0.008646
13	251,6180	-0.000000	-0.000000	-0.000000	-0.047649	-0.010711	-0.009164
14	302,2871	-0.000000	-0.000000	-0.000000	-0.049950	-0.011229	-0.009607
15	357,5674	-0.000000	-0.000000	-0.000000	-0.052325	-0.011763	-0.010063
16	417,4441	-0.000000	-0.000000	-0.000000	-0.054478	-0.012247	-0.010477
17	481,9320	-0.000000	-0.000000	-0.000000	-0.056552	-0.012713	-0.010876
18	551,0267	-0.000000	-0.000000	-0.000000	-0.058906	-0.013242	-0.011329
19	596,5497	-0.000000	-0.000000	-0.000000	-0.060491	-0.013598	-0.011634
20	615,2672	-0.000000	-0.000000	-0.000000	-0.061143	-0.013745	-0.011759
21	634,7631	-0.000000	-0.000000	-0.000000	-0.061934	-0.013923	-0.011911
22	653,5519	-0.000000	-0.000000	-0.000000	-0.062824	-0.014123	-0.012083
23	673,1286	-0.000000	-0.000000	-0.000000	-0.063439	-0.014261	-0.012201



PORT	NON-DIMENSIONAL AREA	N - M	M LR-FT	M/TD	N	L LB	L/T
1	3.7645	-0.000000	-0.000000	-0.000000	-0.002838	-0.000638	-0.000577
2	5.7722	-0.000000	-0.000000	-0.000000	-0.004174	-0.000938	-0.000849
3	10.6480	-0.000000	-0.000000	-0.000000	-0.006816	-0.001532	-0.001386
4	20.1129	-0.000000	-0.000000	-0.000000	-0.009792	-0.002201	-0.001992
5	32.1592	-0.000000	-0.000000	-0.000000	-0.012353	-0.002777	-0.002513
6	46.7867	-0.000000	-0.000000	-0.000000	-0.014632	-0.003289	-0.002976
7	63.9957	-0.000000	-0.000000	-0.000000	-0.016767	-0.003769	-0.003410
8	83.7859	-0.000000	-0.000000	-0.000000	-0.018589	-0.004179	-0.003781
9	106.1575	-0.000000	-0.000000	-0.000000	-0.020231	-0.004548	-0.004115
10	131.1105	-0.000000	-0.000000	-0.000000	-0.021799	-0.004900	-0.004434
11	153.8764	-0.000000	-0.000000	-0.000000	-0.023006	-0.005172	-0.004679
12	194.0306	-0.000000	-0.000000	-0.000000	-0.024632	-0.005537	-0.005010
13	250.6766	-0.000000	-0.000000	-0.000000	-0.026680	-0.005998	-0.005427
14	301.1561	-0.000000	-0.000000	-0.000000	-0.028401	-0.006385	-0.005777
15	356.2246	-0.000000	-0.000000	-0.000000	-0.029903	-0.006722	-0.006082
16	415.8822	-0.000000	-0.000000	-0.000000	-0.031715	-0.007129	-0.006451
17	480.1288	-0.000000	-0.000000	-0.000000	-0.033111	-0.007443	-0.006735
18	548.9645	-0.000000	-0.000000	-0.000000	-0.034402	-0.007733	-0.006997
19	594.3172	-0.000000	-0.000000	-0.000000	-0.034929	-0.007852	-0.007105
20	612.9602	-0.000000	-0.000000	-0.000000	-0.035180	-0.007909	-0.007156
21	631.8900	-0.000000	-0.000000	-0.000000	-0.035350	-0.007948	-0.007192
22	651.1066	-0.000000	-0.000000	-0.000000	-0.035588	-0.008000	-0.007239
23	670.6101	-0.000000	-0.000000	-0.000000	-0.035873	-0.008064	-0.007297

## REFERENCES

1. Margason, Richard J.; and Gentry, Garl L., Jr.: Aerodynamic Characteristics of a Five-Jet VTOL Configuration in the Transition Speed Range. NASA TN D-4812, 1968.
2. Vogler, Raymond P.: Interference Effects of Single and Multiple Round or Slotted Jets on a VTOL Model in Transition. NASA TN D-2380, Aug. 1964.
3. Abbott, W.A.: Studies of Flow Fields Created by Vertical and Inclined Jets when Stationary or Moving over a Horizontal Surface. British ARC C.P. No. 911, 1967.
4. Ziegler, H.; and Wooler, P.T.: Analysis of Stratified and Closely Spaced Jets Exhausting into a Crossflow. NASA CR-132297, Nov. 1973.
5. Gentry, Garl L.; and Margason, Richard J.: Jet Induced Lift Losses on VTOL Configurations Hovering In and Out of Ground Effect. NASA TN D-3166, Feb. 1966.
6. Kuhlman, J.M.; Ousterhout, D.S.; and Warcup, R.W.: Experimental Investigation of Effect of Jet Decay Rate on Jet-Induced Pressures on a Flat Plate. NASA CR-2979, Apr. 1978.
7. Kuhlman, J.M.; Don S. Ousterhout; and Warcup, R.W.: Appendix to Experimental Investigation of Effects of Jet Decay Rate on Jet-Induced Pressures on a Flat Plate: Tabulated Data. NASA CR-158990, Nov. 1978.
8. Kuhlman, J.M.; and Warcup, R.W.: Effects of Jet Decay Rate on Jet-Induced Loads on a Flat Plate. J. Aircraft, Vol. 15, No. 5, May 1978, pp. 293-297.

## REFERENCES

9. Margason, Richard J.: Review of Propulsion-Induced Effects on Aerodynamics of Jet/STOL Aircraft. NASA TN D-5617, Feb. 1970.
10. Vogler, Raymond D.: Surface Pressure Distributions Induced on a Flat Plate by a Cold Air Issuing Perpendicularly from the Plate and Normal to a Low Speed Free-Stream Flow. NASA TN D-1629, Mar. 1963.
11. Fearn, Richard L.; and Weston, Robert P.: The Induced Pressure Distribution of a Jet in a Crossflow. NASA TN D-7916, July 1975.
12. Kamotani, Yasuhiro; and Greber, Isaac: Experiments on a Turbulent Jet in a Cross Flow. NASA CR-72893, June 1971.



1. Report No NASA CR-159004		2. Government Accession No		3. Recipient's Catalog No	
4. Title and Subtitle Experimental Investigation of Jet-Induced Loads on a Flat Plate in Hover Out-of-Ground Effect				5. Report Date February 1979	
				6. Performing Organization Code	
7. Author(s) John M. Kuhlman Ronald W. Warcup				8. Performing Organization Report No	
9. Performing Organization Name and Address Old Dominion University Research Foundation P. O. Box 6369 Norfolk, Virginia 23508				10. Work Unit No	
				11. Contract or Grant No NAS1-14193-40	
12. Sponsoring Agency Name and Address National Aeronautics and Space Administration Washington, DC 20546				13. Type of Report and Period Covered Contractor Report FR, 7/1-12/31/77	
				14. Sponsoring Agency Code	
15. Supplementary Notes Final report for NAS1-14193-40, Mr. Richard J. Margason, Technical Monitor					
16. Abstract  Effects of varying jet decay rate on jet-induced loads on a flat plate located in the plane of the jet exit perpendicular to the jet axis have been investigated using a small-scale laboratory facility. Jet decay rate has been varied through use of two cylindrical centerbodies having either a flat or hemispherical tip, which were submerged various distances below the flat plate-jet exit plane. Increased jet decay rate, caused by the presence of a centerbody or plug in the jet nozzle, led to an increased jet-induced lift loss on the flat plate. Jet-induced lift losses reached 1 percent of the jet thrust for the quickest jet decay rates for plate areas equal to 100 times the effective jet exit area. The observed lift loss versus jet decay rate trend agreed well with results of previous investigations.					
17. Key Words (Suggested by Author(s))  jet VTOL aircraft hover propulsion aerodynamics effects			18. Distribution Statement  Unclassified - Unlimited  Subject Category: <u>02</u>		
19. Security Classif (of this report) Unclassified	20. Security Classif (of this page) Unclassified	21. No of Pages 63	22. Price* \$5.25		

**End of Document**